A Striatal interneuron circuit for continuous target pursuit

Namsoo Kim[1], Haofang E. Li[1], Ryan N. Hughes[1], David Gallegos[2], Anne E. West[2], Il Hwan Kim[3], and Henry H. Yin[1, 2]

[1]Department of Psychology and Neuroscience, Duke University

[2]Department of Neurobiology, Duke University

[3]Department of Psychiatry, Duke University

Correspondence should be addressed to Henry Yin, Box 91050, Duke University, Durham, NC 27708. Email: hy43@duke.edu

Key words: basal ganglia, striatum, medium spiny neuron, fast-spiking interneuron

Most adaptive behaviors require precise and continuous tracking of targets in space. We studied the contribution of a striatal microcircuit to target pursuit using a novel continuous pursuit task in freely moving mice. We show that, in the sensorimotor striatum, many parvalbumin-positive fast-spiking interneurons (FSIs) represent the distance between self and target. On the other hand, the striatal projection neurons (SPNs), which receive FSI projections, more commonly represent self-velocity during pursuit behavior. Moreover, FSIs are shown to regulate SPN activity during pursuit, so that movement velocity is continuously modulated by distance to target. Long-term silencing or transient optogenetic manipulation of FSI output can selectively pursuit behavior. Our results reveal a key role of this striatal interneuron circuit in pursuit behavior, suggesting that it is used to convert distance error signals into velocity commands, allowing the animal to use target distance to guide pursuit behavior.

Introduction

Whether pursuing a prey or approaching a mate, many natural behaviors involve continuous tracking of targets in space. Yet the neural substrates of such behavior remain poorly understood. While previous studies have examined pursuit of moving targets in head-fixed monkeys, implicating a network of brain areas including the cerebellum, frontal cortex, and basal ganglia (Basso et al., 2005; Krauzlis, 2004; Lisberger et al., 1987; O'Driscoll et al., 2000), technical limitations have prevented the study of natural pursuit behavior in freely moving animals. To study it properly requires continuous monitoring of both the animal and the target, while recording neural activity of specific neuronal populations in order to elucidate their functional contributions. We designed a novel behavioral task, in which freely moving mice follow a continuously moving target. Using 3D motion capture, we were able to track not only the position of the animal but also the distance to target, a crucial variable for accurate pursuit.

We studied the contribution of the inhibitory interneuron circuit in the sensorimotor striatum to pursuit behavior. The striatum is a major basal ganglia nucleus that has been implicated in action initiation and selection (Mink, 1996), compulsive behavior (Monteiro and Feng, 2015), and habit formation (Yin and Knowlton, 2006). The sensorimotor striatum is characterized by the highest expression of parvalbumin positive GABAergic FSIs, which receives glutamatergic inputs from the cerebral cortex and provides feedforward inhibition of the much more numerous striatal projection neurons (SPNs)(Gage et al., 2010; Tepper et al., 2010). Reduced number of FSIs is associated with neuropsychiatric disorders such as Tourette's syndrome and obsessive-compulsive disorder (Burguière et al., 2013; Kalanithi et al., 2005). Studies also implicated the FSIs in choice behavior and habitual lever pressing (Gage et al., 2010; O'Hare et al., 2017). Nevertheless, the computations performed by the FSI-SPN circuit remain obscure.

Recent work has shown that sensorimotor SPN activity is often highly correlated with movement velocity (Kim et al., 2014; Yttri and Dudman, 2016), and stimulation of striatal output frequency-dependently determines movement velocity (Bartholomew et al., 2016). Yet it remains unclear how, during target-driven pursuit behavior, the striatal output is commanded by representation of distance to target. We hypothesize that FSI-SPN interneuron circuit plays a critical role in pursuit behavior, allowing cortical inputs representing the spatial relationship

between self and target to reach the basal ganglia and guide action selection. In particular, projections from FSIs to SPNs convert a distance representation from the cortex to constant adjustments in velocity commands. To test this hypothesis, we used wireless *in vivo* electrophysiology, calcium imaging, and cell-type specific manipulation of neural activity to examine the contributions of the striatal microcircuit to pursuit behavior in freely moving mice. Our results established for the first time a key role of this local striatal circuit in pursuit behavior.

RESULTS

Pursuit task and motion capture

To elucidate mechanisms underlying pursuing behaviors, we developed a continuous pursuing task in which freely moving mice follow a moving sucrose spout. Head and target positions were recorded at 100 Hz (**Figure 1A-B**). Mice were first water deprived and trained for 6-10 sessions, each lasting 15 min. All mice rapidly increased the time spent following the target (**Figure S1A**). Constant velocity (16 mm/s) and variable velocity (5-48 mm/s) conditions were used to assess pursuit performance.

Because in our task pursuit behavior is self-initiated, we separated periods in which the mice were following the target and periods in which they were not. 'Following' is defined as staying in a spatially defined zone close to the target for at least 800 ms, when the mouse head is next to the sucrose spout ((<15 mm x-axis, <10 mm in y axis, <20 mm in z axis). Behavior from the rest of the session is classified as 'not following' (Constant velocity, **Figures 1C-E**; variable velocity, **Figures S1B-D**). Mice spent most of the time during the session following the moving target (Constant velocity: 66.0 ± 3.5 % following; variable velocity: 66.7 ± 5.8 % following**)**. In addition, distance to target is much greater when the mice were not following (Constant velocity: 6.4 ± 0.32 mm, following; 13.5 ± 0.60 mm, not following, **Figure 1D**; variable velocity: 5.5 ± 0.47 mm following and 12.3 ± 0.63 mm not following **Figures S1C**). Self-velocity is also lower during following for the Constant velocity: 18.8 ± 1.03 mm/s, following; 24.0 ± 1.58 mm/s, following, **Figure 1E**; but not for the variable velocity condition: 19.6 ± 2.04 mm/s, following; 22.3 ± 3.12 mm/s, not following **Figures S1D**).

In pursuit behavior, the key variable used to guide self-velocity is distance to target. Mice performed well in both constant and variable velocity conditions, suggesting that variability in target velocity does not affect pursuit performance. Mice could easily adjust their velocity in order to maintain the appropriate distance to target. Velocity can vary while distance is kept relatively constant. To investigate the temporal relationship between these two continuous variables during pursuit, we performed a cross-correlation analysis (constant velocity, **Figure 1F;** variable velocity, **Figure S1E**). With distance as the reference variable, a positive lag means that distance leads velocity, in support of the hypothesis that the distance representation is used to guide velocity. This is exactly what we found. More importantly, this lag measure is positively correlated with the distance error, the key measure of pursuit performance. That is to say, the worse the pursuit performance, the more self-velocity lags self-target distance. We also found that self-velocity increases as distance to target increases, but only during following (**Figures 1G and S1F**). This finding also suggests that mice use distance information to generate the appropriate velocity. In order to perform well on the pursuit task, it is necessary to update distance representation constantly and quickly, using it to drive velocity commands.

Distinct striatal representations of self-target distance and self-velocity

To elucidate how striatal neurons contribute to pursuit behavior, we recorded striatal neurons while mice performed the task. A total of 453 striatal neurons were recorded from 24 mice. Fast spiking interneuron (FSI) or spiny projection neuron (SPN) have markedly different average firing rates and spike waveforms. We were therefore able to classify them using these criteria. We were able to identify 362 putative SPNs in the dorsolateral striatum (trough to peak width: 570.8 ± 2.3 μs, firing rate: 2.1 ± 0.1 Hz) and 91 FSIs (width: 173.9 ± 4.9 μs, firing rate: 20.4 ± 0.9 Hz, **Figure S4A-B and Table 1**). The proportion of FSIs is much higher than expected from anatomical studies (1-2%) because these neurons have much higher firing rates compared to SPNs. Due to their low firing rates, often SPNs are too quiet to be detected or included for data analysis.

To examine the relationship between neural activity and behavior, we calculated correlation between striatal neurons and distance, velocity, acceleration, reward delivery

(**Figures S2 and S3**). Only neurons with high correlations with the relevant behavioral variable were used for subsequent analysis ($r^2 > 0.56$, $P < 0.0001$).

On the whole, FSIs and SPNs showed distinct representations of behavioral variables: FSIs more commonly represented self-target distance (56%) whereas SPNs (32%) more commonly represented velocity (chi square = 88.71, $P < 0.0001$, **Tables 1 and 2**).

As shown in **Figure 2,** there are two distinct populations of SPNs (**Table 1**). One population increases firing as leftward velocity increases (**Figure 2A-C)** and the other increases firing as rightward velocity increases (**Figure 2D-F).** These two populations are summarized in **Figure 2G**. They are direction-specific, symmetric, and the population vector is nearly perfectly correlated with velocity. For comparison, correlation with other variables is much lower (velocity: $r^2 = 0.72 \pm 0.007$; distance: $r^2 = 0.29 \pm 0.022$; acceleration: $r^2 = 0.17 \pm 0.016$, and reward: $r^2 = 0.01 \pm 0.002$, **Figure 2H**). Because these different variables are correlated with each other, low correlation with neural activity cannot be interpreted unambiguously. For time-varying variables like velocity and position, it is impossible for neurons to be correlated with one but not the other. However, very high correlations can tell us which variables are being represented because accurate representations are needed for good pursuit performance. We only considered a neuron to be correlated with a particular behavioral variable if the r^2 value is above 0.56 and higher than alternative variables. **Figure S2A-B** shows a representative neuron and different variables used for the correlation analysis. **Figure 2I** shows that the correlation with velocity is reduced when the mice are not following, for both populations of velocity-correlated neurons. Figure **S2C** show the population activity showing that both left and right velocity variables is drastically reduced when the animal is not following.

Many FSIs (n = 51) showed continuous representation of target distance (**Figure 3, Table 2**). Their firing rates varied monotonically with target distance. The representation of target distance is independent of target or self-movement direction (whether leftward or rightward). One group increases firing as left distance increases (**Figure 3A-C**), whereas a second group increases firing as right distance increases (**Figure 3D-F**). Distance neurons show higher correlation with distance ($r^2 = 0.82 \pm 0.009$) than velocity ($r^2 = 0.36 \pm 0.034$), acceleration ($r^2 = 0.29 \pm 0.032$), and reward ($r^2 = 0.01 \pm 0.002$, **Figure 3H**). **Figure S3A-B** shows a representative neuron and different variables used for the correlation analysis. There is a strong

linear relationship between the population activity of distance FSIs and distance (**Figure 3G**, Left distance: $r^2 = 0.98$, Right distance: $r^2 = 0.99$). For both populations, the mean firing rate corresponds to roughly the 'straight ahead' condition. For the 'left+' neurons, the highest firing rate is reached at the leftmost extreme and lowest firing rate at the rightmost extreme, and vice versa for the 'right+' neurons. **Figure 3I** shows that the correlation with distance is significantly reduced when the mice are not following. Figure **S3C** shows that the correlation between population activity and distance is drastically reduced when the animal is not following.

Optotagging FSIs

Because the striatum contains many different types of neurons, classification of a relatively rare class like the FSI based purely on firing rate and spike waveform may not be reliable. There are other interneurons, such as somatostatin-expressing low-threshold spiking neurons that also have higher rates than SPNs (Tepper et al., 2010). To confirm our classification, we used optrodes to selectively stimulate and record PV+ FSIs at the same time. We injected a Cre-dependent channelrhodopsin (DIO-ChR2) in transgenic mice that express Cre-recombinase in parvalbumin-positive neurons (PV-Cre mice, n = 6 males) and implanted optrodes with both recording electrodes and optic fiber. We used photo-stimulation to identify PV+ FSIs neurons during recording (**Figure 4A**). Only neurons that are activated by light stimulation with short latency (< 8 ms) are classified as FSIs (**Figure 4B, Table 3**). The results support our classification criteria, as the 'optotagged' cells show similar waveforms and firing rates as those we classified as FSIs (**Figure S4A**). More importantly, the identified FSIs also show correlation with distance to target (**Figure 4C-E**, distance: $r^2 = 0.81 \pm 0.018$, velocity: $r^2 = 0.41 \pm 0.085$, acceleration: $r^2 = 0.24 \pm 0.080$, and reward: $r^2 = 0.03 \pm 0.017$). These optogenetically identified FSIs also showed lower correlation with distance when the mice are not following (**Figure 4F**).

In vivo calcium imaging

To confirm our *in vivo* electrophysiological results, we used calcium imaging with miniaturized endoscopes to record FSI activity. We expressed GCaMP6s, a genetically encoded

calcium indicator, in PV+ neurons (injecting the viral vector containing DIO-GCaMP6s in PV-Cre mice). After virus injection, we implanted gradient index (GRIN) lens into the sensorimotor striatum (**Figures 4G and S4C**). We identified 37 FSIs (5 mice, left: n = 4, right: n = 1, **Table 4**). Consistent with our electrophysiology results, we found many FSIs whose activity represents distance (**Figure 4H-I, S4D**). In addition, FSIs also showed a linear relationship with distance to target, with two opponent populations (**Figure 4J**, Left distance: $r^2 = 0.95$, Right distance: $r^2 = 0.71$). Distance PV FSI shows much higher correlation with distance (**Figure 4K**, Left distance: n =15, $r = -0.91 \pm 0.009$; right distance: n = 4, $r = 0.84 \pm 0.027$), $r^2 = 0.80 \pm 0.019$) than velocity ($r^2 = 0.27 \pm 0.055$), acceleration ($r^2 = 0.12 \pm 0.025$), and reward ($r^2 = 0.06 \pm 0.016$). Correlation also greatly reduced when the mice are not following the target (**Figure 4L**, following: $r^2 = 0.80 \pm 0.019$, not following: $r^2 = 0.28 \pm 0.056$).

Suppressing FSI activity selectively impairs pursuit performance

These results show that distance to target, the key variable in pursuit behavior, is represented by striatal FSI neurons. However, they do not tell us whether this representation is required for successful pursuit. To test necessity, we silenced FSIs using the tetanus toxin light chain (TeLC). TeLC can prevent neurotransmitter release by cleaving its vesicle associated membrane protein 2 (Murray et al., 2011; Schiavo et al., 1992). Because the FSIs are known to express parvabumin (PV), we used Cre-dependent TeLC (AAV-flex-TeLC) in mice that express Cre recombinase in PV-positive neurons (PV-Cre).

We first trained mice on the pursuit task. We then injected AAV-flex-TeLC into the sensorimotor striatum of PV-Cre mice (control: n = 6; TeLC: n = 7, **Figure 5A**), thus expressing TeLC in a cell type- and region-specific manner (**Figures 5B, S5A, and S5B**). Following recovery, we tested the mice again. FSI silencing markedly disrupted target pursuit performance, reducing the amount of time spent following the target (control: 36.1 ± 4.6 %; TeLC: 15.2 ± 3.8 %, **Figure 5C**). The distance was marginally increased (control: 13.2 ± 0.8 mm; TeLC: 17.0 ± 1.7 mm, t-test, p = 0.087, **Figure 5D**). However, this effect is specific to pursuit behavior, as it did not impair overall movement velocity (control: 16.4 ± 0.4 mm/s TeLC: 15.7 ± 1.4 mm/s, **Figure 5E**) during the session.

TeLC effects are permanent and it can be difficult to rule out compensatory plasticity due to reduced FSI synaptic transmission. We therefore used designer receptors exclusively activated by designer drugs (DREADDs) to suppress FSI activity reversibly (**Figure 5F**). We injected an AAV vector encoding a Cre-dependent designer G protein-coupled hM4Di receptor bilaterally into the SENSORIMOTOR of PV-Cre mice (control n = 6, DIO-hM4D n = 6, **Figures 5G, S5C and S5D**). Injection of the synthetic ligand clozapine-N-oxide (CNO) for the hM4Di receptor reduced the amount of time spent following the target (control: 77.5 ± 3.2 %; DIO-hM4D: 43.7 ± 8.0 %, **Figure 5H**), increasing distance (control: 6.9 ± 1.12 mm; DIO-hM4D: 10.5 ± 1.10 mm, **Figure 5I**) without affecting movement velocity in general (control: 10.7 ± 0.5 mm/s DIO-hM4D: 13.1 ± 0.5 mm/s, **Figure 5J**).

Optogenetic manipulation of FSI activity

Finally, to test the effects of acute and temporally specific manipulation of FSI activity, we performed optogenetic experiments using channelrhodopsin and halorhodopsin during pursuit behavior (Boyden et al., 2005; Zhang et al., 2007). First, FSIs was excited by photo-stimulation using DIO-ChR2 injected in the sensorimotor striatum of PV-Cre mice (**Figures 6A and S6A; control = 3 mice; DIO-ChR2 = 4 mice**). This could result in the inhibition of SPNs (**Figure S7**). Photo-stimulation increased distance error (**Figure 6B-C**). Velocity was also decreased during photo-activation of FSI, and then increased immediately after the termination of stimulation (**Figure 6D**). These results were also observed using a shorter pulse train (200 ms, **Figure S6B**). However, there was no effect on the overall proportion of time following (control: 65.6 ± 4.3 %; DIO-ChR2: 77.7 ± 2.3 %, **Figure 6E**) or on overall movement velocity (control: 17.76 ± 1.4 mm/s; DIO-ChR2: 18.3 ± 0.5 mm/s, **Figures 6F, S6C-D**).

In contrast, FSI firing was decreased by halorhodopsin (**S6E**). Photo-stimulation also increased distance error (**Figure 6H-I,** control = 4 mice; DIO-eNpHR3.0 = 6 mice). However, velocity was increased by photo-stimulation, and decreased after stimulation (**Figure 6J**). A similar pattern was observed using 200 ms stimulation (**Figure S6F**). However, there was no effect on the overall proportion of time following (control: 72.2 ± 5.8 %; DIO-eNpHR3.0: 79.9 ± 3.0 %, **Figure 6K,**) or on movement velocity in general (control: 17.5 ± 1.0 mm/s; DIO-eNpHR3.0: 19.7 ± 1.0 mm/s, **Figures 6L and S6G-H**). Thus, while artificial manipulation of

FSI activity with channelrhodopsin or halorhodopsin both acutely disrupted pursuit performance, as measured by distance error, they do so in opposite ways. FSI activation reduced self-velocity, while FSI inhibition increased self-velocity (compare **Figure 6D** with **6J**).

Working model of how FSI-SPN circuit contributes to pursuit

Based on the anatomical organization of the FSI-SPN circuit and our results, we proposed a working model for how this circuit contributes to pursuit behavior in our task. According to this model (**Figure 7**), the SPNs and FSIs that form a functional unit share excitatory cortical inputs, yet the FSI provides strong inhibition of some SPNs and disinhibition of others (**Figure S7A-B**). This is mainly a summary of the known anatomy of the feedforward inhibition circuit, yet our model sheds light on this organization. We propose that signals representing target distance can be sent via the corticostriatal projections to FSIs and SPNs. The GABAergic output of a FSI sends a temporally delayed and inverted version of this signal to the relevant SPNs. Consequently, a given velocity SPN can receive two inputs, one net positive signal from the cortex that represents distance, and a slightly delayed version of the same input from the FSI that is subtracted from the excitatory input because the FSI-SPN projection is inhibitory (**Figure 7A**). The output of the SPN will then reflect the difference between excitatory cortical input and a temporally delayed version of the same signal. This 'temporal difference' signal is then used as a velocity command to drive performance.

Such a model is supported by our data. A key feature of the model is that FSI activity reflects a delayed version of the distance representation. If we use a slightly delayed (100 ms) version of the distance measure as the Distance $_{t}$ signal, and FSI output as the Distance $_{t-1}$ signal, then by performing a simple subtraction we can obtain the difference that reflects the velocity command from the SPN (**Figure 7B**). This operation is similar to taking the time derivative of the distance representation. Our working model is supported not only by the known anatomy but also by actual data from simultaneously recorded FSI-SPN pairs with the same direction (left distance FSI and leftward velocity SPN). As shown by **Figure 7C-E**, model output is remarkably similar to the actual firing rate of the SPN.

Population coherence is also increased during pursuit (**Figure S7C**). Coherence is a measure of the correlation between two signals as a function of frequency. We found that in the delta (0-3 Hz) and alpha (8-12 Hz) range, coherence between different neuronal populations was increased (SPN-SPN, FSI-SPN, and FSI-FSI).

DISCUSSION

To successfully pursue a moving target, it is necessary not only to regulate velocity and direction of movement but also to monitor continuously the distance between self and target. Here we showed for the first time that mice use internal representations of such a distance variable to guide their pursuit behavior. We showed that mice use distance information to guide self-velocity during pursuit (**Figure 1F**), and that the FSI-SPN circuit is critical for converting change in distance into velocity commands. In particular, FSIs in the sensorimotor striatum preferentially represent target distance, and are also necessary for successful pursuit performance. They send inhibitory projections to SPNs, which preferentially represent velocity.

In our task, the target always moves from side to side, each cycle consisting of both leftward and rightward movements. During pursuit, the target could be on either side of the mouse. We identified distinct types of self-target distance representations in FSIs. Some neurons increase firing when the target moves to the left side of the animal, and decrease firing when it moves to the right, and vice versa for other neurons (**Figure 3**). On the other hand, SPNs are strongly correlated with movement velocity, with clear direction-specificity (**Figure 2**). This result is broadly in agreement with previous work (Cui et al., 2013; Kim et al., 2014; Panigrahi et al., 2015; Tecuapetla et al., 2014; Yttri and Dudman, 2016).

When the animal is not pursuing, it could be engaged in any number of activities, including grooming, orienting, rearing, and so on. It is not surprising that, under these conditions, the neural representations of the relevant variables are degraded and the correlation between firing rate and the relevant variable is lower. This reduction in correlation when the mouse is not pursuing is especially dramatic for FSI distance neurons (**Figure 3I**).

Although velocity and distance are both continuous, time-varying variables, there are key differences between them. Movement velocity can be detected by mainly proprioceptive and vestibular sensory inputs (Yin, 2014). At rest velocity is close to zero, consistent with the usually low firing rates of SPNs (Wilson, 2004). On the other hand, FSIs are characterized by high tonic

firing rates, which make them more suitable for signaling the distance variable. Our results suggest that tonic FSI firing close to the middle of the range is used to represent the effective zero, when the target is directly in front of the mouse. Both negative and positive errors are represented by FSIs, by increasing and decreasing from the tonic baseline value (**Figure 3G**). For example, for neurons that increase firing when the target is to the left, the left extreme correspond to the highest firing rate and the right extreme corresponds to the lowest firing rate, and vice versa for neurons that increase firing when target is on the right side. One possibility is that the two types of FSIs project to distinct functional classes of SPNs. 'Too much to the left' would suppress rightward neurons and activate leftward SPNs, whereas too much to the right would suppress leftward and activate rightward SPNs. Thus, bidirectional control is enabled by FSIs, in which increase and decrease from a tonic baseline. Different types of errors (left vs. right) are indicated by the sign of the signal in relation to the effective zero. This feature is also found in downstream structures in the substantia pars reticulata (Barter et al., 2015b).

The critical role of the FSI-SPN circuit in pursuit is further supported by our experiments using cell-type specific manipulations. These manipulations all impaired pursuit performance without affecting overall movement per se. For example, blocking transmitter release in FSIs with TeLC did not affect movement velocity, but reduced the time spent following the target. Inhibiting FSIs with DREADD or halorhodopsin increased pursuit error, suggesting that the distance-related signals provided by FSIs are necessary for pursuit behavior. While halorhodopsin and channelrhodopsin both increased self-target distance (pursuit error), they produced opposite effect on self-velocity.

In **Figure 7** we describe a working model of the pursuit behavior based on our results. We propose that the feedforward inhibition circuit is similar to a 'differentiator' circuit. The difference between the present distance representation and the last distance representation one time step ago drives the SPN. This comparison process generates the velocity command in a given direction. A positive difference means that distance error has increased, i.e. the target is farther away, and velocity must be increased accordingly to reduce the distance error. Thus during pursuit, an increase in left distance naturally leads to an increase in the temporal difference signal computed by the FSI-SPN circuit, and a corresponding increase in the leftward velocity command. A negative difference signal indicates that the distance error is decreasing

and velocity in that direction should be reduced. SPN output is therefore regulated by the *change* in distance between self and target in real time.

In order to obtain the high correlation between neural activity and behavior observed in this study, three conditions are necessary: 1) high temporal and spatial resolution in kinematic measures are required. It is particularly important to obtain the *direction* of movement. 2) The task must be designed so that the behavior of a freely moving animal remains relatively simple. 3) Rather than measuring behavior as discrete events, it is necessary to measure and analyze it as a continuous process. The relevant behavioral variables are time-varying continuous signals, not discrete time stamps.

We previously reported strong correlations between SPNs and direction-specific head velocity in freely moving mice (Kim et al., 2014). Recent studies showed similar results (Panigrahi et al., 2015; Rueda-Orozco and Robbe, 2015), though they did not examine correlation between time-varying neural activity and kinematic variables. The key innovation in the current study is the introduction of the continuous pursuit task, which allows us to quantify a key variable—distance to target—that is necessary for successful performance.

A recent paper concluded that FSIs are not needed for behavioral performance but for 'action selection' learning (Owen et al., 2018). But our study leads to a different conclusion: FSIs are critical for performance. Owens et al show that FSI silencing impairs learning on a 3-nose poke sequence task and egocentric/allocentric learning. Both tasks would require targeting of discrete spatial locations. But in their study behavior is measured as conventional time stamps. There is no continuous measure as behavior is assumed to consist of discrete task-related events, and neural activity is aligned to these events. While Owens et al. are correct to argue that FSIs are not critical for behavior per se, their behavioral measure did not reveal the key function of the FSI-SPN circuit in pursuit behavior. It is possible that the significant learning defects they observed following disruption of FSI output can be explained by performance deficits which their measures were not sensitive enough to detect. For example, if the FSI-SPN circuit is disrupted, mice would have trouble approaching the target, on either their spatial sequence task or their egocentric/allocentric orienting task. Both require appropriate guidance of the head toward a spatial target, a function that, according to the present study, requires the FSI-SPN circuit. Thus continuous and careful quantification of behavior is critical in

revealing the contribution of specific neural circuits. Conventional measures of either performance or learning are often inadequate.

We also found that neurons representing distance and velocity are largely independent of reward delivery. This result is in accord with previous work showing that the correlation between nigrostriatal activity and movement velocity is similar on both reward and punishment trials (Barter et al., 2015a; Kim et al., 2014). Although some studies have suggested that sensorimotor striatal neurons are modulated by reward, they did not monitor continuous behavioral variables or establish a time-varying relationship between neural activity and reward consumption or detection(Isomura et al., 2013). Our results cannot be explained by predicted reward value because we found two opponent populations of distance FSIs for distinct distance errors, which are spatially defined (left and right). It is possible, however, that other striatal regions, such as the limbic and associative areas, are more critical for reward prediction and processing (Yin et al., 2008).

It remains unclear how the two types of distance FSIs are connected with downstream SPNs. Both SPNs and FSIs are known to receive convergent inputs from different cortical regions(Berke, 2011; Gerfen and Wilson, 1996; Ramanathan et al., 2002). Based on our results, we hypothesize that these inputs can provide information on distance to target (Hintiryan et al., 2016). An obvious candidate is the use of visual representations from visual cortical areas, but the relevant signals could be multi-modal, involving visual, auditory, and vestibular inputs, all of which reach the striatum (Hintiryan et al., 2016). Future research will be needed to identify the source of corticostriatal signals to the striatal interneuron circuit and to elucidate how representations of self-target relationships are formed upstream.

In conclusion, we showed for the first time that the FSI-SPN circuit performs an important computational function in pursuit behavior. This circuit can regulate self-velocity during pursuit using continuous updating of distance to target. Given the ubiquity of approaching a spatially discrete target in the natural behavior of diverse organisms and the evolutionary conservation of the basal ganglia circuits, these results have significant implications for our understanding of how neural circuits implement voluntary behavior. Finally, it should be noted that, although the FSI-SPN circuit is critical for pursuit performance on our task, that does not mean it is the only circuit used for pursuit. Other circuits, especially those in the cerebellum,

may also be important (Lisberger et al., 1987). It is possible that the basal ganglia and cerebellum have complementary functions in pursuit behavior: the basal ganglia are critical for general guidance, and the cerebellum may be critical for rapid and precise targeting. Future studies will be needed to understand the distinct contributions of these different areas to pursuit.

METHODS

Animals. All experimental procedures were approved by the Animal Care and Use Committee at Duke University. *In vivo* recording experiments used male and female C57BL/6J purchased from Jackson labs. For TeLC and halorhodopsin experiments, Parvalbumin-Cre mice (Pvalb-2A-Cre-D, Jackson Labs stock #012358) were used. For DREADD experiments, *Drd1a*-tdTomato:: *PV*-Cre mice were used. *Drd1a*-tdTomato reporter mice were generated in the Calakos lab (RRID: IMSR_JAX:016204)(Ade et al., 2011). A total of 18 mice were used for *in vivo* electrophysiological recording experiments, 13 mice for TeLC experiments, 12 mice for DREADD experiments, and 10 mice for halorhodopsin experiments. All mice were between 3-8 months old. They were maintained on a 12:12 light cycle and tested during the light phase. The mice used for electrophysiology experiments were singly housed. All other mice were group housed. During all behavioral experiments, the mice had restricted access to water and food. After each training and recording session, they had free access to water for ~ 30 minutes and ~3 g of home chow. Their weights were maintained at 85-90% of their initial weights.

Wireless *in vivo* electrophysiology. A total of 24 C57BL/6J mice aged were used in the electrophysiology experiments (17 males and 7 females). Custom-built 16- channel microwire arrays were used. The arrays consisted of micro-polished tungsten wires, 35 μm in diameter and 4-5 mm in length, in a 2 by 8 configuration, and attached to an Omnetics connector (Omnetics Connector Corporation). To implant the electrode arrays, each mouse was fully anesthetized with isoflurane (induction at 3%, maintained at 1%), and head-fixed on a stereotax (Kopf). Meloxicam (2 mg/kg) was administered subcutaneously after anesthesia induction and prior to surgery for pain relief. Detailed surgery procedure for electrode implant was previously described (Fan et al., 2012; Rossi et al., 2013). The stereotaxic coordinates are (mm relative to Bregma): AP + 0.4 mm, ML ±2.4 mm, DV -2.3 mm. The electrode arrays were grounded to screws placed in the skull using a silver ground wire, and then anchored in place with dental

acrylic. Following the surgeries, all mice were allowed to recover for at least two weeks before the recording experiments. Single-unit activity was recorded with a miniaturized wireless headstage (Triangle Biosystems) and a Cerebus data acquisition system (Blackrock), as described previously (Fan et al., 2011). Data were filtered with analog and digital band-pass filters (analog high-pass 1st order Butterworth filter at 0.3 Hz, analog low-pass 3rd order Butterworth filter at 7.5 kHz), and then separated with a high-pass digital filter (4th order Butterworth filter at 250 Hz) and sampled at 30 kHz. The data was processed using online sorting algorithms and then re-sorted offline (Offline Sorter, Plexon). Waveforms were classified as single units as previously described (Rossi et al., 2013). The following criteria were used: 1) a signal to noise ratio of at least 3:1; 2) consistent waveforms throughout the recording session; 3) refractory period of at least 800 μs.

***In vivo* calcium imaging.** Each mouse (PV-Cre, n = 5) was unilaterally injected with 500 nl of AAV-EF1a-DIO-GCamp6s (Stanford virus core) into dorsolateral striatum (Bregma +0.4, +- 2.4; -2.3) every 0.2 mm from 3.0 mm using a Nanoject III injector (Drummond Scientific, USA) at a rate of 1 nl per second. The injection pipette was left in place for 10 min post-injection before it was retracted. After viral injection, a gradient index (GRIN) lens (Inscopix: 1 mm x 9 mm, n = 3; UCLA Miniscope, 1.8 mm x 4.3 mm, n =2) was implanted in the dorsolateral striatum directly above the injection site after aspirating ~2 mm of the above cortical tissue with 21-gauge blunt needle. Once in place, the lens was secured to the skull using a liquid dental cement and covered with Kwik-Sil to protect the lens surface. Two weeks after the GRIN lens implantation, the baseplate (Inscopix or UCLA Miniscope) was mounted onto the mouse head under visual guidance to determine the best field of view. All recorded movies of calcium activity were initially preprocessed in Mosaic (Inscopix) for motion correction and spatial binning (5 x 5 for Inscopix; 4 x 4 for miniscope, and subsequently analyzed using custom MATLAB scripts. We used constrained non-negative matrix factorization (CNMF) for simultaneously denoising, deconvolving, and demixing of calcium imaging data (Pnevmatikakis et al., 2016). This method allows accurate source extraction of cellular signals (Zhou et al., 2017).

Behavior task and analysis. The moving reward target is a sucrose spout moved by a stepper motor from left to right relative to the mouse standing on a platform (Bipolar, 56.3 x 56.3 mm, DC 1.4A, 2.9Ω, 1.8 degree / step, Oriental motor, USA). The stepper motor was controlled using

MATLAB (Mathworks). Two infrared reflective markers (6.35 mm diameter) were used for tracking mouse and target movements. One marker was located on the wireless recording headstage and another was placed approximately 20 mm from the sucrose spout. These markers were captured by eight Raptor-H Digital Cameras (Motion analysis, CA, 100 Hz sampling rate). The data was transformed into Cartesian coordinates (x, y and z) by the Cortex program (Motion Analysis, CA). Matlab communicated with Cortex program (Motion Analysis) online to control reward delivery. Reward (~12 ul of 20% sucrose) was delivered every 800 ms during following. Prior to the recording sessions, all mice were trained until they followed the target consistently (2-4 hours of training over 1 week). In most experiments, the target moved at a constant velocity (16 mm/s). On some sessions, however, target velocity was varied randomly (5-48 mm/s, updated every 2 ms by MATLAB).

Analysis of neural activity and movement. For correlation analysis, we first obtained rate histogram data in 10 ms bins. For FSIs, a 200 ms Gaussian filter was used for smoothing. For SPNs, a 50 ms Gaussian filter was used for smoothing. Correlation with each of the different behaviorally relevant variables (distance, velocity, and acceleration, and reward delivery) was computed. For reward correlation, neural and reward times were aligned by self rightward movement from –3.5 s (left) to 3.5 s (right) at 50 ms bin. Using different peri-event windows does not change the results. We compared the automatically computed correlation coefficients for different behavioral variables. A neuron is considered to be correlated with a particular behavioral variable if the absolute value of r is higher than 0.75 and higher than the r values for alternative variables.

TeLC experiments. Cre-inducible adeno-associated viral (AAV) plasmids containing GFP-tagged TeLC or GFP alone, each with the reading frame inverted in a flip-excision (FLEX) cassette (AAV-FLEX-TeLC and AAV-FLEX-GFP) were originally obtained from Dr. Peer Wulff, Christian Albrechts University, Kiel, Germany (Murray et al, 2011), and the AAV vector was generated by the University of Pennsylvania vector core facility in serotype AAV2/5. We first implanted cannulae in PV-Cre mice (n = 13, 24 gauge, 3-mm length below pedestal, Plastics One). Cannulae were secured in place with skull screws and dental acrylic. A stylet was

inserted and protruded ~0.2 mm beyond the end of each cannula. The mice then trained daily for ~10 days, each session consisting of 200 side to side movements of the target. To inject the virus (0.5ul of either TeLC-GFP or GFP virus), the stylets were removed, and virus was infused through custom made 31 gauge steel injectors extending ~0.5 beyond the tip of the guide cannulae at 0.1ul/min for 5 min. The injector was kept in the brain for at least 5 min for diffusion. Coordinates for all injections relative to bregma were as follows: AP + 0.4 mm, ML ±2.4 mm, DV -2.3 mm (Paxinos and Franklin, 2003). Approximately 3 weeks after surgery, the mice were tested on the pursuit task again.

DREADD experiments. The *CAG*-FLEX-*rev*-hM4D:2a:GFP plasmid was provided by Scott Sternson (Addgene #52536). UNC Viral Vector Core packaged this plasmid into AAV 2/5 and also provided AAV2/5-EF1a-DIO-EYFP (titers > 1 x 10^{12} particles/mL). The hM4Di virus (n = 6) or EYFP virus (n = 6) injected into the sensorimotor striatum of *Drd1a*-tdTomato:: *PV*-Cre mice. Small craniotomies were made over the injection sites and 1.0 µL of virus was delivered bilaterally to dorsolateral striatum via a Nanoject II (Drummond Scientific) at a rate of 0.1 µL/min. The injection pipette was held in place for 5 minutes following injection and then slowly removed. Coordinates for all injections relative to bregma were as follows: AP: + 0.8 mm, ML: ± 2.7 mm, DV: 3.2 mm. Mice were allowed a minimum of 3 weeks before behavioral training. The behavioral procedure is the same as described above, except mice were first tested on 100 cycles of target motion. This pre-injection period establishes the baseline performance measures for each mouse, before given injection of the synthetic ligand clozapine-N-oxide (CNO) for the hM4Di receptor. CNO was dissolved to 10 mg/mL in DMSO and diluted in PBS solution to administer 5 mg/kg per mouse with a maximum injection volume of 0.5 mL. The same volume of PBS/DMSO solution was used as the control vehicle injection. 30 minutes after control or CNO injection, the mice were tested again for 100 cycles.

Optogenetics. Halorhodopsin (AAV5-EF1a-DIO-eNpHR3.0-EYFP) and channelrhodopsin (AAV5-EF1a-DIO-ChR2) were acquired from University of North Carolina at Chapel Hill vector core. The halorhodopsin and channelrhodopsin viruses (0.5ul each side) was injected using the same procedure as described above for the DREADD experiments using the following

coordinates: AP + 0.4 mm, ML ±2.4 mm, DV -2.8 mm. Both heterozygous males and female PV-Cre mice were used (n = 17). We then implanted an optic fiber just above the site of injection (DV -2.3 mm) on one side and an optrode on the other side to measure *in vivo* neural activity during halorhodopsin and channelrhodopsin activations. The optrode was a custom made microwire array (4-mm, 4 x 4 tungsten) with an optic fiber attached to the lateral side and angled so the cone of the emitted light encompassed the electrode tips (Sparta et al., 2012). Control mice received bilateral implants of optic fibers only. For optrode recordings, tethered setup was used using the Cerebus data acquisition system (Blackrock). Before testing each day, mice were connected to a 2-m sheathed fiber (105-μm core diameter, 0.22 NA) with a ceramic sleeve (Precision Fiber Products). The fiber was connected to a 532 nm or 470 nm DPSS laser (Shanghai Laser & Optics). The laser was controlled with MATLAB (MathWorks). Before the experimental session, the final output of the laser was adjusted, based on the transmittance of each implant, to be 8-15 mW into the brain. Photo-stimulation (500 ms) was delivered 3.2 s after at least 800 ms of following. If the mouse continues to follow, stimulation was delivered every 3.2 s. Each session contained 200 cycles of the moving target.

Histology. After the completion of all behavioral tests, the mice with chronically implanted electrode arrays were deeply anesthetized with isoflurane and transcardially perfused with 0.9% saline followed by 10% buffered formalin solution. Coronal brain sections (80 μm) were sliced using a Vibratome 1000 Plus, stained with thionin, and examined with a light microscope to verify location of the electrode tips within the striatum. Mice infected by AAV5-Ef1a-Flex-NpH3.0-eYFP (Halorhodopsin), AAV5-CBA-Flex-TelC-GFP, or AAV5-CAG-Flex-hM4D-2A-GFP (DREADD) were deeply anesthetized with isoflurane, perfused transcardially with Tris buffered saline (TBS; pH 7.4) containing 25 U/ml heparin, followed by 4% paraformaldehyde (PFA) in TBS. Perfused brains were removed, post-fixed overnight at 4°C in 4% PFA, and then cryo-protected with 30% sucrose in TBS for 48 hrs. Brains were cut into 50 μm coronal sections using a cryostat (Leica CM 3000), and treated with blocking solution (TBS containing 5% normal goat serum and 0.2% Triton X-100) for 2 hr and incubated overnight at 4°C with chicken anti-GFP monoclonal antibody (1:500; abcam; ab13970). After washing three times with TBST (TBS containing 0.2% Triton X-100), sections were incubated with goat anti-chicken Alexa

Fluor® 488 IgG (1:500; invitrogen; A11039) overnight at 4°C. Sections were counterstained with a 4',6-diamidino-2-phenylindole solution (DAPI; Sigma-Aldrich). After washing four times, the sections were cover slipped with FluorSave (CalBioChem) aqueous mounting medium. Whole brain section images were taken by tile scan imaging using a LSM 710 confocal microscope (Zeiss) with a 10x objective. To observe individual neurons expressing Halorhodopsin, TelC, or DREADD in the striatum, a 20x objective lens with 3× digital zoom was used.

Statistics. Statistical analysis was performed using Matlab and Graphpad Prism. No statistical methods were used to predetermine sample size. All statistical tests were two-tailed. To determine the effects of FSI inactivation, we used two-way repeated measures ANOVAs. Post hoc tests were performed whenever there was a significant interaction.

Data and code availability. All data and Matlab codes used in the present study are available upon request.

References

Ade, K.K., Wan, Y., Chen, M., Gloss, B., and Calakos, N. (2011). An Improved BAC Transgenic Fluorescent Reporter Line for Sensitive and Specific Identification of Striatonigral Medium Spiny Neurons. Front Syst Neurosci *5*, 32.

Barter, J., Li, S., Lu, D., Rossi, M., Bartholomew, R., Shoemaker, C.T., Salas-Meza, D., Gaidis, E., and Yin, H.H. (2015a). Beyond reward prediction errors: the role of dopamine in movement kinematics. Frontiers in Integrative Neuroscience *9*, 39.

Barter, J.W., Li, S., Sukharnikova, T., Rossi, M.A., Bartholomew, R.A., and Yin, H.H. (2015b). Basal ganglia outputs map instantaneous position coordinates during behavior. Journal of Neuroscience *35*, 2703–2716.

Bartholomew, R.A., Li, H., Gaidis, E.J., Stackmann, M., Shoemaker, C.T., Rossi, M.A., and Yin, H.H. (2016). Striatonigral control of movement velocity in mice. Eur J Neurosci *43*, 1097-1110.

Basso, M.A., Pokorny, J.J., and Liu, P. (2005). Activity of substantia nigra pars reticulata neurons during smooth pursuit eye movements in monkeys. European Journal of Neuroscience *22*, 448-464.

Berke, J.D. (2011). Functional properties of striatal fast-spiking interneurons. Frontiers in systems neuroscience *5*.

Boyden, E.S., Zhang, F., Bamberg, E., Nagel, G., and Deisseroth, K. (2005). Millisecond-timescale, genetically targeted optical control of neural activity. Nat Neurosci *8*, 1263-1268.

Burguière, E., Monteiro, P., Feng, G., and Graybiel, A.M. (2013). Optogenetic stimulation of lateral orbitofronto-striatal pathway suppresses compulsive behaviors. Science *340*, 1243-1246.

Cui, G., Jun, S.B., Jin, X., Pham, M.D., Vogel, S.S., Lovinger, D.M., and Costa, R.M. (2013). Concurrent activation of striatal direct and indirect pathways during action initiation. Nature *494*, 238-242.

Fan, D., Rich, D., Holtzman, T., Ruther, P., Dalley, J.W., Lopez, A., Rossi, M.A., Barter, J.W., Salas-Meza, D., Herwik, S.*, et al.* (2011). A wireless multi-channel recording system for freely behaving mice and rats. PLoS One *6*, e22033.

Fan, D., Rossi, M.A., and Yin, H.H. (2012). Mechanisms of action selection and timing in substantia nigra neurons. J Neurosci *32*, 5534-5548.

Gage, G.J., Stoetzner, C.R., Wiltschko, A.B., and Berke, J.D. (2010). Selective activation of striatal fast-spiking interneurons during choice execution. Neuron *67*, 466-479.

Gerfen, C.R., and Wilson, C.J. (1996). The basal ganglia. In Handbook of chemical neuroanatomy, L.W. Swanson, A. Bjorklund, and T. Hokfelt eds. (Amsterdam, Elsevier), pp. 371-468.

Hintiryan, H., Foster, N.N., Bowman, I., Bay, M., Song, M.Y., Gou, L., Yamashita, S., Bienkowski, M.S., Zingg, B., Zhu, M.*, et al.* (2016). The mouse cortico-striatal projectome. Nat Neurosci *19*, 1100-1114.

Isomura, Y., Takekawa, T., Harukuni, R., Handa, T., Aizawa, H., Takada, M., and Fukai, T. (2013). Reward-modulated motor information in identified striatum neurons. The Journal of Neuroscience *33*, 10209-10220.

Kalanithi, P.S., Zheng, W., Kataoka, Y., DiFiglia, M., Grantz, H., Saper, C.B., Schwartz, M.L., Leckman, J.F., and Vaccarino, F.M. (2005). Altered parvalbumin-positive neuron distribution in basal ganglia of individuals with Tourette syndrome. Proc Natl Acad Sci U S A *102*, 13307-13312.

Kim, N., Barter, J.W., Sukharnikova, T., and Yin, H.H. (2014). Striatal firing rate reflects head movement velocity. Eur J Neurosci *40*, 3481-3490.

Krauzlis, R.J. (2004). Recasting the smooth pursuit eye movement system. J Neurophysiol *91*, 591-603.

Lisberger, S.G., Morris, E., and Tychsen, L. (1987). Visual motion processing and sensory-motor integration for smooth pursuit eye movements. Annual review of neuroscience *10*, 97-129.

Mink, J.W. (1996). The basal ganglia: focused selection and inhibition of competing motor programs. Progress in neurobiology *50*, 381-425.

Monteiro, P., and Feng, G. (2015). Learning from Animal Models of Obsessive-Compulsive Disorder. Biol Psychiatry.

Murray, A.J., Sauer, J.F., Riedel, G., McClure, C., Ansel, L., Cheyne, L., Bartos, M., Wisden, W., and Wulff, P. (2011). Parvalbumin-positive CA1 interneurons are required for spatial working but not for reference memory. Nat Neurosci *14*, 297-299.

O'Driscoll, G.A., Wolff, A.L., Benkelfat, C., Florencio, P.S., Lal, S., and Evans, A.C. (2000). Functional neuroanatomy of smooth pursuit and predictive saccades. Neuroreport *11*, 1335-1340.

O'Hare, J.K., Li, H., Kim, N., Gaidis, E., Ade, K., Beck, J., Yin, H., and Calakos, N. (2017). Striatal fast-spiking interneurons selectively modulate circuit output and are required for habitual behavior. eLife *6*.

Owen, S.F., Berke, J.D., and Kreitzer, A.C. (2018). Fast-Spiking Interneurons Supply Feedforward Control of Bursting, Calcium, and Plasticity for Efficient Learning. Cell *172*, 683-695 e615.

Panigrahi, B., Martin, K.A., Li, Y., Graves, A.R., Vollmer, A., Olson, L., Mensh, B.D., Karpova, A.Y., and Dudman, J.T. (2015). Dopamine Is Required for the Neural Representation and Control of Movement Vigor. Cell *162*, 1418-1430.

Paxinos, G., and Franklin, K. (2003). The mouse brain in stereotaxic coordinates (New York, Academic Press).

Ramanathan, S., Hanley, J.J., Deniau, J.M., and Bolam, J.P. (2002). Synaptic convergence of motor and somatosensory cortical afferents onto GABAergic interneurons in the rat striatum. J Neurosci *22*, 8158-8169.

Rossi, M.A., Fan, D., Barter, J.W., and Yin, H.H. (2013). Bidirectional Modulation of Substantia Nigra Activity by Motivational State. PloS one *8*, e71598.
Rueda-Orozco, P.E., and Robbe, D. (2015). The striatum multiplexes contextual and kinematic information to constrain motor habits execution. Nature neuroscience.
Schiavo, G., Benfenati, F., Poulain, B., Rossetto, O., Polverino de Laureto, P., DasGupta, B.R., and Montecucco, C. (1992). Tetanus and botulinum-B neurotoxins block neurotransmitter release by proteolytic cleavage of synaptobrevin. Nature *359*, 832-835.
Sparta, D.R., Stamatakis, A.M., Phillips, J.L., Hovelsø, N., van Zessen, R., and Stuber, G.D. (2012). Construction of implantable optical fibers for long-term optogenetic manipulation of neural circuits. Nature protocols *7*, 12-23.
Tecuapetla, F., Matias, S., Dugue, G.P., Mainen, Z.F., and Costa, R.M. (2014). Balanced activity in basal ganglia projection pathways is critical for contraversive movements. Nature communications *5*.
Tepper, J.M., Tecuapetla, F., Koos, T., and Ibanez-Sandoval, O. (2010). Heterogeneity and diversity of striatal GABAergic interneurons. Front Neuroanat *4*, 150.
Wilson, C.J. (2004). Basal ganglia. In The synaptic organization of the brain, G.M. Shephard, ed. (New York, Oxford University Press).
Yin, H.H. (2014). Action, time and the basal ganglia. Philosophical Transactions of the Royal Society B: Biological Sciences *369*.
Yin, H.H., and Knowlton, B.J. (2006). The role of the basal ganglia in habit formation. Nat Rev Neurosci *7*, 464-476.
Yin, H.H., Ostlund, S.B., and Balleine, B.W. (2008). Reward-guided learning beyond dopamine in the nucleus accumbens: the integrative functions of cortico-basal ganglia networks. Eur J Neurosci *28*, 1437-1448.
Yttri, E.A., and Dudman, J.T. (2016). Opponent and bidirectional control of movement velocity in the basal ganglia. Nature *533*, 402-406.
Zhang, F., Wang, L.P., Brauner, M., Liewald, J.F., Kay, K., Watzke, N., Wood, P.G., Bamberg, E., Nagel, G., Gottschalk, A*., et al.* (2007). Multimodal fast optical interrogation of neural circuitry. Nature *446*, 633-639.

Acknowledgements: We would like to thank Justin O'Hare and Nicole Calakos for their help with DREADD experiments, Koji Toda and Dongye Lu for help with 3D printing, and Mark Rossi for helpful comments on the manuscript. This research was supported by grants from the National Institutes of Health (R01 DA040701 and R01MH112883 to HHY, and R01DA033610 to AEW). The authors declare that there is no conflict of interest regarding the publication of this article.

Author Contributions: NK and HHY designed the experiments. NK, HEL, DG, and IK conducted experiments. NK and HHY analyzed the data and wrote the manuscript.

Video 1. Representative 3D motion capture of a mouse during pursuit behavior (following).

Video 2. Representative 3D motion capture of a mouse that is not following the target (same mouse as in Video 1).

Video 3. Representative calcium imaging signals using a miniaturized endoscope.

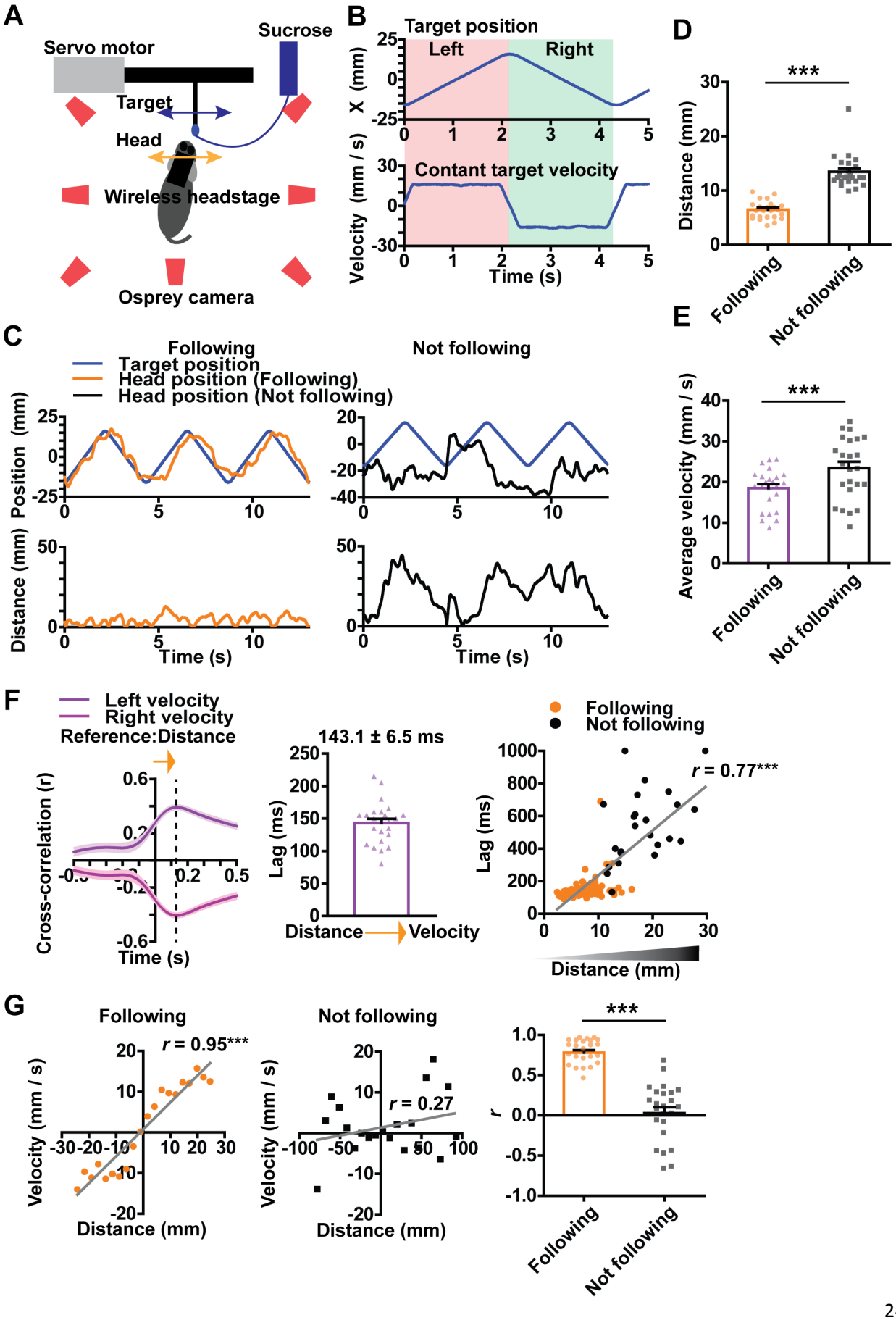

Figure 1. Summary of behavioral results

A) Illustration of the pursuit task and location of the infrared cameras for 3D motion capture. The target moves continuously from side to side. **B)** Position and velocity traces of the target, which moves along the x-axis at a constant velocity of 16 mm/s (see **Figures S1** for variable velocity condition). The total distance traveled from left to right is 32 mm. Thus, it takes the target about 2 seconds to move from one extreme to another. **C)** Representative traces of mouse head and target position during a session. Left panel shows the head and target positions during 'Following'. 'Following' is defined as a period in which the head is close to the target (<15 mm x-axis, <10 mm in y axis, <20 mm in z axis). Right panel shows the head and target positions during 'Not following'. Also see **Videos 1 and 2** for examples**. D)** Distance is significantly shorter during following (paired t-test, $t(23) = 10.31$, $p < 0.0001$). Error bars indicate ± s.e.m. *** $p < 0.0001$. **E)** Average self-velocity is significantly lower during following (paired t-test, $t(23) = 6.53$, $p < 0.0001$). **F)** Illustration of the temporal relationship between distance and self-velocity. Cross correlation analysis reveals the lag between these two variables, showing that distance leads self-velocity during pursuit behavior. In addition, the lag shows a positive correlation with distance ($r = 0.77$, $p < 0.0001$). When the mouse is actively pursuing and maintaining a small distance, the lag between distance and velocity is small, but the lag increases as pursuit performance declines. **G**) Self-velocity as a function of distance to target (pursuit error). Mice appear to use distance information to generate the appropriate velocity only during following ($p < 0.0001$).

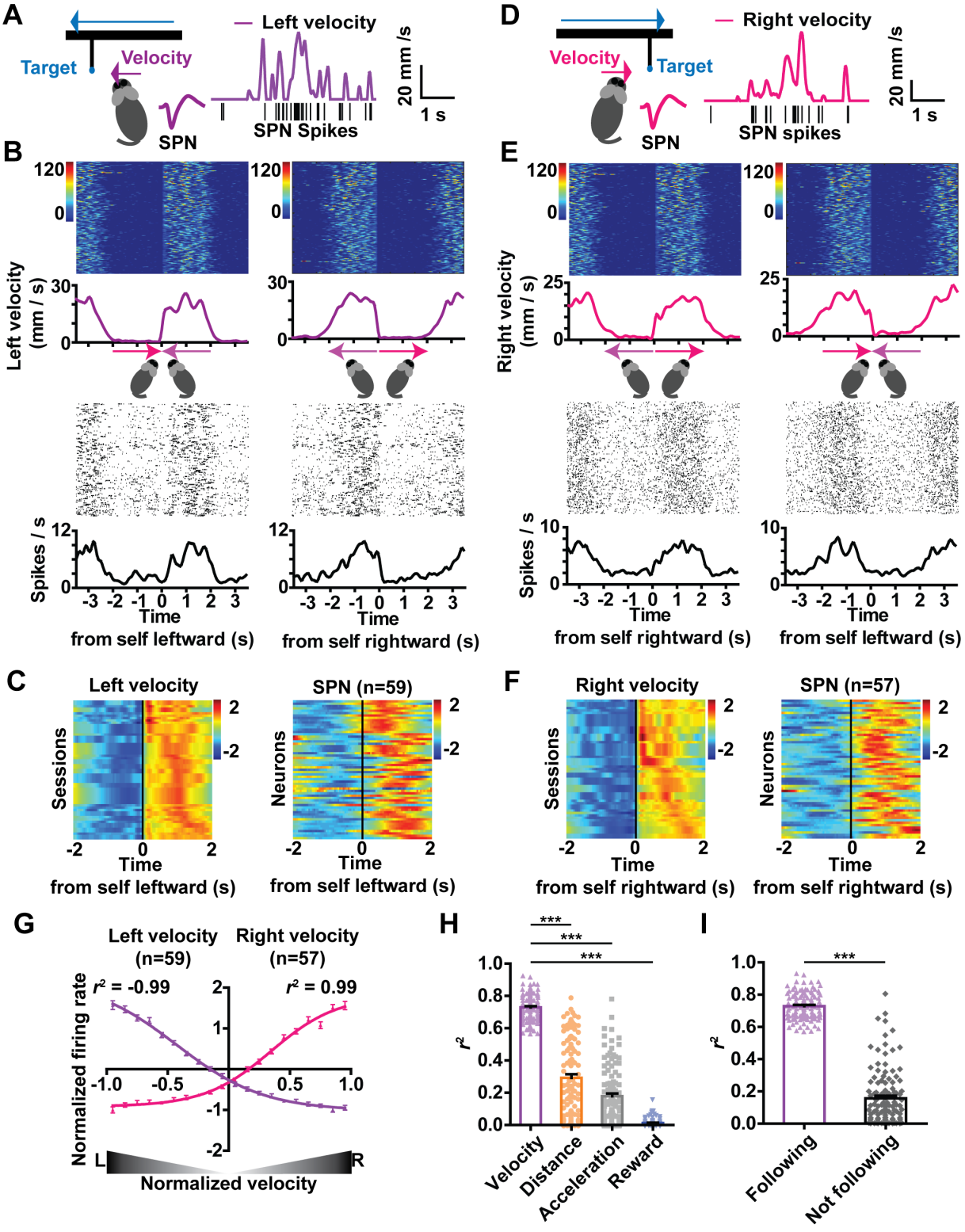

Figure 2. SPNs represent self velocity

A) Representative left velocity SPN and spike waveform. The firing rate of this neuron is positively correlated with leftward velocity. **B)** Representative left velocity SPN. Time zero is the start of leftward or rightward. Note the similarity between time-varying velocity measure and spike raster plots. **C)** Spike density function of all left velocity SPNs (z-scored values). Each row represents average velocity measure and the firing rate measure of corresponding SPNs from a single session. Note that some rows in the velocity plot are identical, because multiple neurons are correlated with the same kinematic variable. **D)** Representative right velocity SPN and spike waveform. The firing rate of this neuron is positively correlated with rightward velocity. **E)** Representative right velocity SPN. Time zero is the start of rightward or leftward movement. Note the similarity between time-varying velocity measure and spike raster plots. **F)** Spike density function of all right velocity SPNs (z-scored values). **G)** Population summary of all velocity-correlated SPNs. The relationship between neural activity and velocity is best described by a sigmoid function. **H)** The correlation coefficients between firing rate of velocity SPNs and alternative behavioral variables. In each case, velocity has the highest coefficient of correlation with firing rate (repeated measures ANOVA $F(3,463) = 453.8$, $p < 0.0001$; Bonferroni post-hoc: velocity vs. distance $p < 0.0001$, velocity vs. acceleration $p < 0.0001$, velocity vs. reward $p < 0.0001$). Error bars indicate ± s.e.m. *** $p < 0.0001$. **I)** Velocity SPNs show weaker correlation if the mouse is not following (paired t-test, $p < 0.0001$).

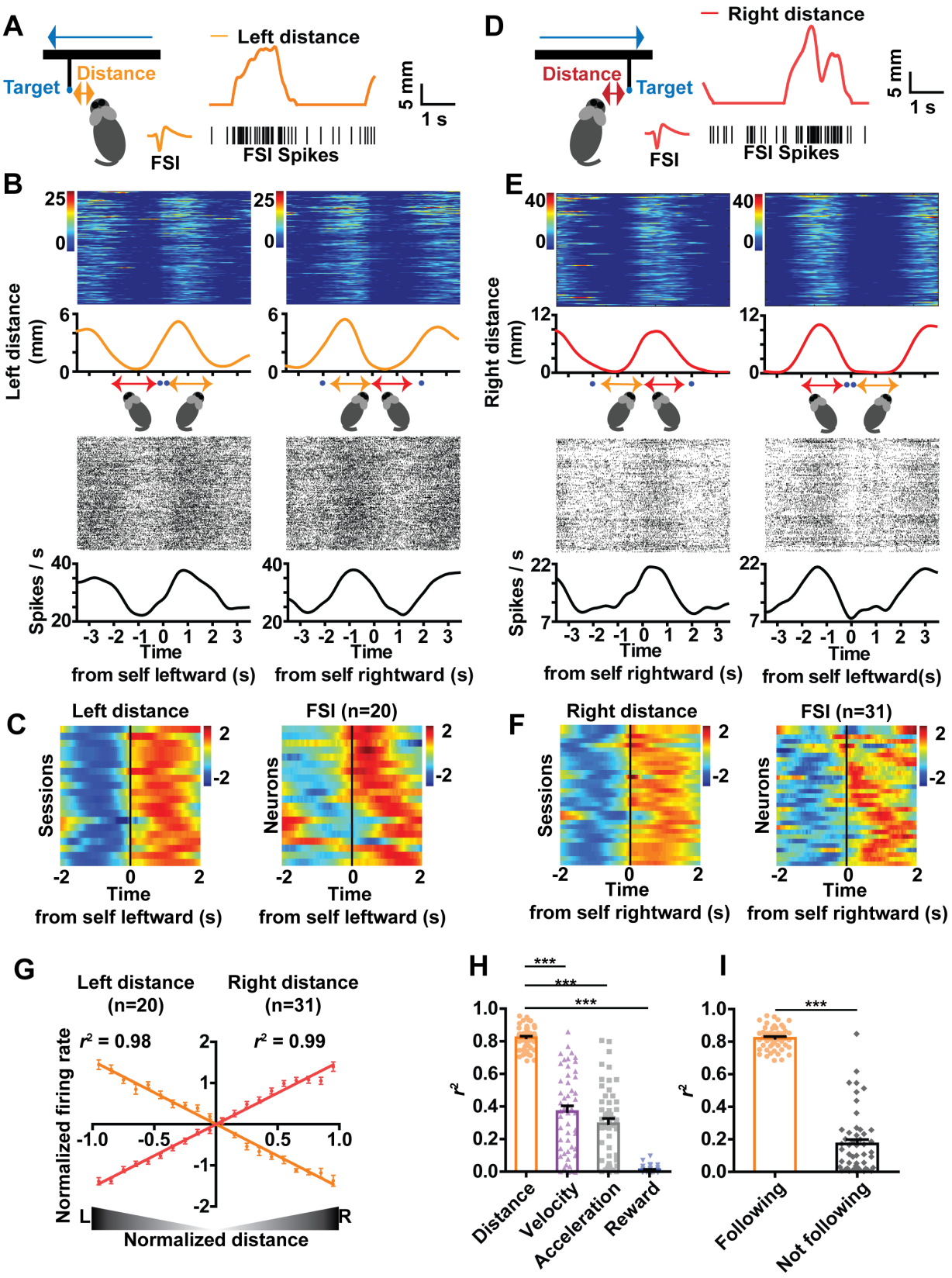

Figure 3. FSIs can represent distance to target

A) Representative left distance FSI. The firing rate of this neuron is positively correlated with distance to target on the left side of the head, regardless of whether the mouse is moving leftward or rightward. **B)** Representative left distance FSI. The firing rate of this neuron is proportional to leftward distance. Time zero is the start of leftward or rightward pursuit. **C)** Spike density function of all left distance FSIs. Each row represents average distance measure and the firing rate measure of corresponding FSI from a single session. Note that some rows in the velocity plot are identical, because multiple neurons are correlated with the same kinematic variable. **D)** Representative right distance FSI. The firing rate of this neuron is proportional to distance to target on the left side of the head, regardless of whether the mouse is moving leftward or rightward. **E)** Representative right distance SPN and spike waveform. The firing rate of this neuron is positively correlated with target distance on the right side. Time zero is the start of leftward or rightward pursuit. **F)** Spike density function of all right distance FSIs. **G)** Population summary of all distance-correlated FSIs. **H)** The correlation coefficients between firing rate of distance FSIs and alternative behavioral variables. In each case, distance has the highest coefficient of correlation with firing rate (repeated One-way ANOVA $F(3,203) = 193.0$, $p < 0.0001$; Bonferroni post-hoc: distance vs. velocity $p < 0.0001$, distance vs. acceleration $p < 0.0001$, distance vs. reward $p < 0.0001$). Error bars indicate ± s.e.m. *** $p < 0.0001$. **I)** Distance FSIs show much weaker correlation when not following (paired t-test, $p < 0.0001$).

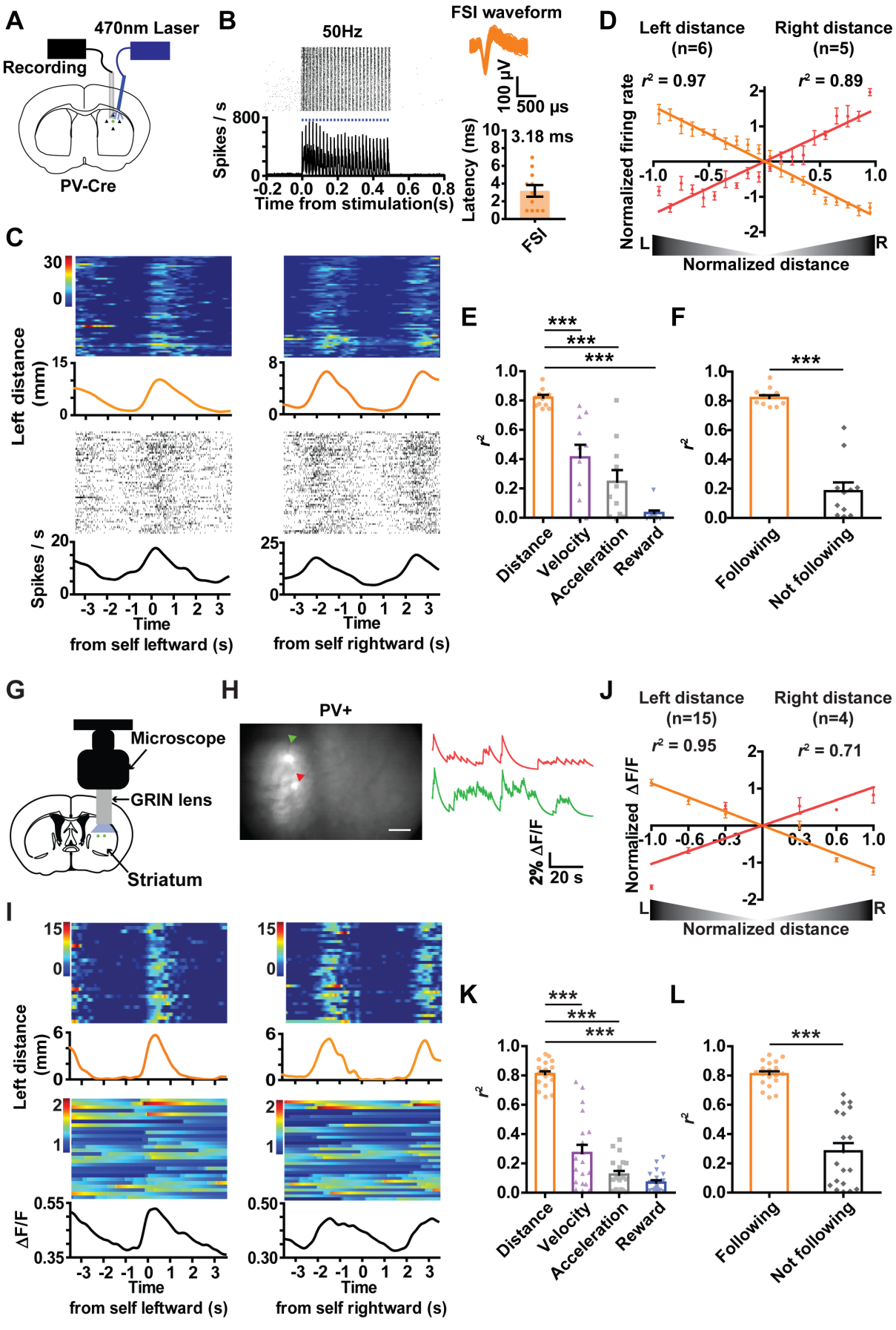

Figure 4. Optotagging and In vivo calcium imaging of FSI activity during pursuit

A) Schematic illustration of simultaneous stimulation and recording using a chronically implanted optrode. An AAV vector with Cre-inducible ChR2 is injected into the sensorimotor striatum of PV-Cre mice. **B)** A representative left distance neuron that is optically tagged. ChR2-induced stimulation at 50 Hz reliably triggered spiking in FSIs with a short latency (average latency = 3.18 ± 0.65 ms). **C)** Representative left distance FSI that is optically tagged. The firing rate of this neuron is proportional to leftward distance. Time zero is the start of leftward or rightward pursuit. **D)** Population summary of all optotagged distance FSI neurons. **E)** Correlation between optotagged distance FSIs and different behavioral variables (repeated One-way ANOVA $F(3,43) = 30.98$, $p < 0.0001$; Bonferroni post-hoc: distance vs. velocity $p < 0.0001$, distance vs. acceleration $p < 0.0001$, distance vs. reward $p < 0.0001$). Error bars indicate ± s.e.m. *** $p < 0.0001$. **F)** Correlation between FSI distance neurons and distance is significantly lower when the animal is not actively pursuing the target (paired t-test, $p < 0.0001$). **G)** Calcium imaging with an implantable GRIN lens. Schematic illustration of the GRIN lens implant. A Cre-dependent GCamp6s virus was injected into the sensorimotor striatum of PV-Cre mice. **H)** Representative image of FSIs. Red and green traces indicate two simultaneously imaged FSIs. Because FSIs are rare, only 2-11 cells are recorded per mouse. Also see **Video 3**. **I)** Representative left distance FSI. Calcium signal from this neuron is proportional to leftward distance. Time zero is the start of leftward or rightward pursuit. **J)** Population summary of all distance FSIs. **K)** Correlation between distance FSIs and different behavioral variables (repeated One-way ANOVA, $F(3,75) = 103.4$, $p < 0.0001$; Bonferroni post hoc analysis: distance vs. velocity $p < 0.0001$; distance vs. acceleration $p < 0.0001$; distance vs. reward $p < 0.0001$). **L)** Correlation between FSI distance neurons and distance is significantly lower when the animal is not actively pursuing the target (paired t-test, $p < 0.0001$)

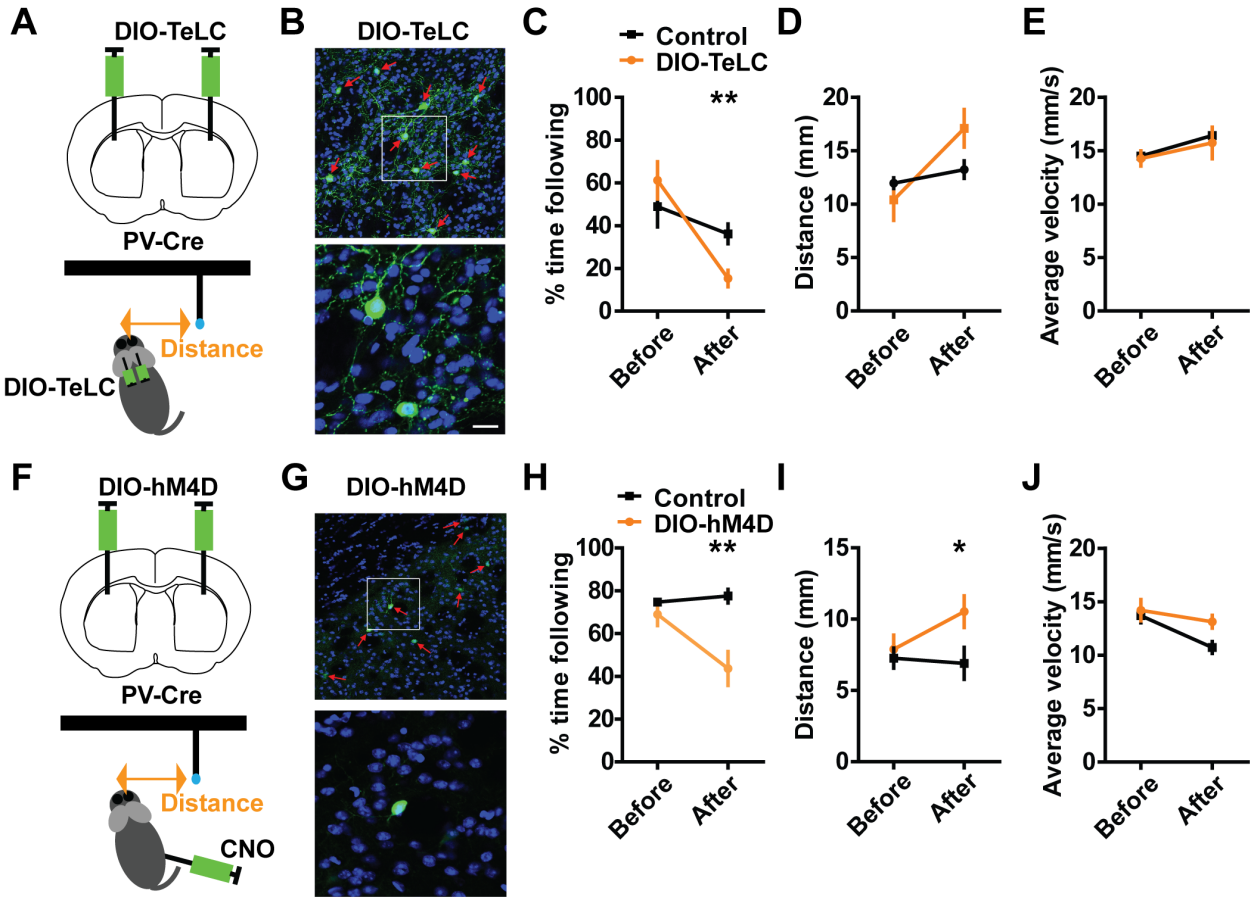

Figure 5. Silencing FSI activity disrupts pursuit performance

A) To silence neural activity in FSIs, we injected the Cre-dependent DIO-TeLC virus into the striatum of PV-Cre mice. TeLC silences neurons by cleaving the vesicular associated membrane protein 2 and preventing transmitter release **B)** GFP staining showing FSIs infected with GFP-tagged TeLC, (control: n = 6, DIO-TeLC: n = 7). **C)** Duration of self-initiated pursuit behavior (% time spent following) is significantly reduced by TeLC. A repeated measures ANOVA revealed a significant interaction: $F(1,11) = 6.88$, $p = 0.024$. Post hoc test showed a significant effect of TeLC ($p = 0.0051$). Error bar indicates ± s.e.m. ** $P < 0.01$. **D)** Distance error is greater in the TeLC group compared to the Control group (GFP only). Repeated measure ANOVA: Interaction: $F(1,11) = 5.92$, $P < 0.05$. Post hoc unpaired t-test, $p = 0.09$. **E)** TeLC did not affect velocity: no significant interaction: $F(1,11) = 0.08$, $P = 0.77$, no effect of Time, $F(1,11) = 12.73$, $P = 0.05$, or of Group: $F(1,11) = 0.94$, $P = 0.67$. **F)** To reversibly inactivate FSIs, we injected the Cre-dependent DIO-hM4D virus into the striatum. **G)** GFP staining showing FSIs in the striatum infected with GFP-tagged DREAAD (control: n = 6, DIO-hM4D: n = 6). **H)** hM4Di reduced % time spent following the target. There was a significant interaction: $F(1,10) = 15.2$, $P = 0.0030$. Postdoc test revealed a significant effect of CNO after injection ($P = 0.0028$). **$P < 0.01$. Error bar indicates ± s.e.m. **I)** hM4Di increased distance: Interaction: $F(1,10) = 9.26$, $P = 0.044$. * $P < 0.05$. **J)** hM4Di did not affect velocity. No interaction: $F(1,10) =$

5.11, P = 0.12, main effect of time: $F(1,10) = 23.21$, $P < 0.01$, no effect of Group: $F(1,10) = 12.09$, $P = 0.11$).

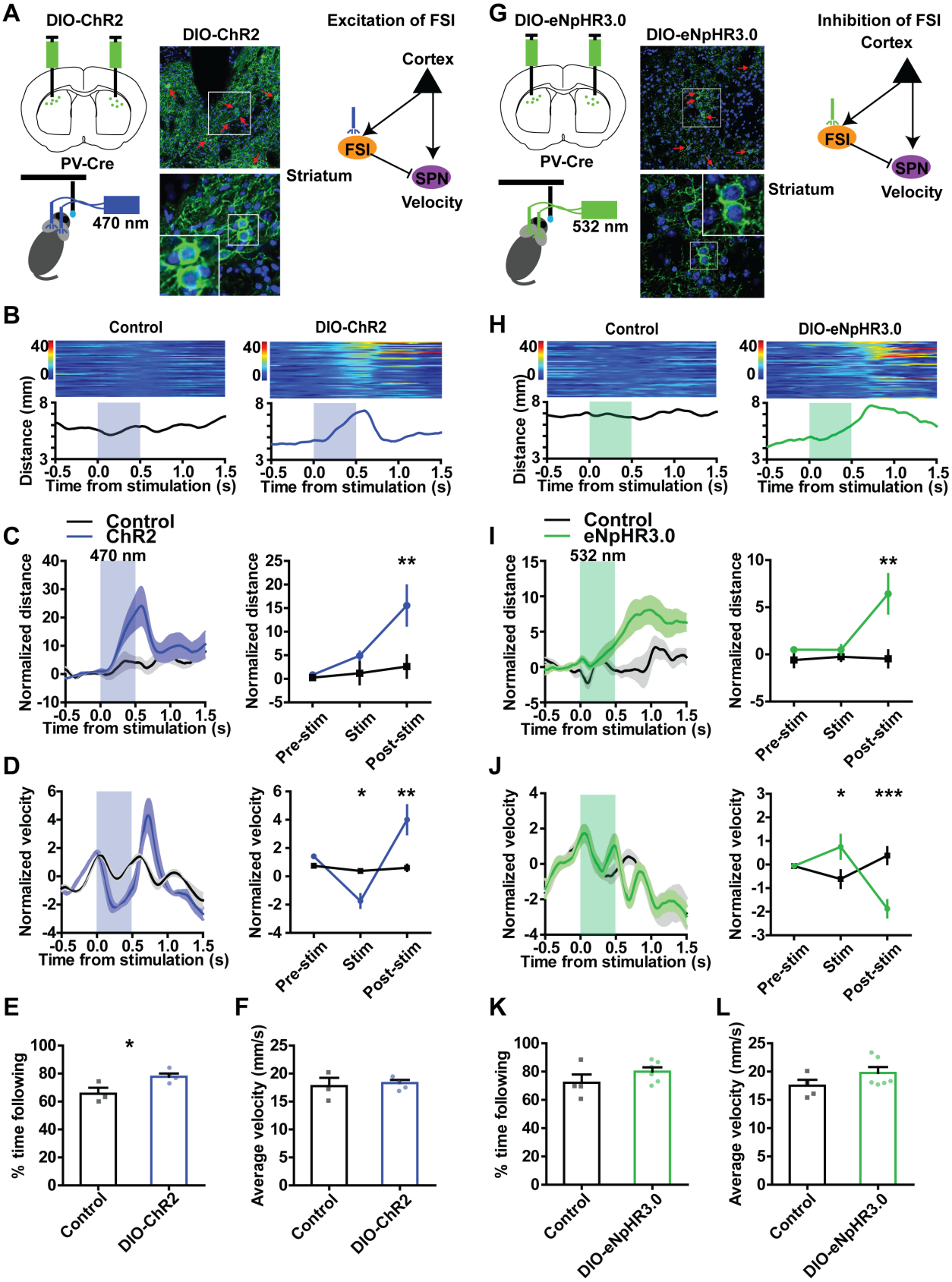

Figure 6. Optogenetic manipulation of FSI activity disrupts pursuit performance

A) To manipulate FSI firing rate in vivo, we injected Cre-dependent channelrhodopsin into the sensorimotor striatum of PV-Cre mice. GFP staining showing FSIs in the striatum infected with channelrhodopsin (AAV-EF1a-DIO-ChR2-EYFP) (fiber only PV-Cre control: n = 3, DIO-ChR2: n = 4). **B**) A representative control mouse and DIO-ChR2 mouse. Only DIO-ChR2 mice showed transiently increased distance as a result of photo-stimulation (500 ms) during pursuit. **C)** Population summary data. Distance error is increased by photo-stimulation. Stimulation significantly altered distance error (repeated measures two-way ANOVA, Interaction: $F(2,10) = 4.673$, $p < 0.05$, Time: $F(2,10) = 8.708$, $p < 0.01$, Group: $F(1.10) = 5.821$, $p = 0.06$; Boferroni post-hoc: Pre-stim NS, Stim NS, Post-stim $p < 0.01$). Error bar indicates ± s.e.m. ** $P < 0.01$. **D)** DIO-ChR2 group shows reduced velocity during photo-stimulation and increased velocity after photo-stimulation. Control shows no change Repeated two-way ANOVA, Interaction: $F(2,10) = 9.010$, $p < 0.01$, Time: $F(2,10) = 10.63$, $p < 0.01$, Group: $F(1.10) = 8.150$, $p < 0.05$, Boferroni post-hoc: Pre-stim NS, Stim $p < 0.05$, Post-stim $p < 0.01$, * $P < 0.05$. **E)** Stimulation slightly increased % time spent following ($p = 0.04$). **F)** Stimulation had no effect on average velocity ($p = 0.71$). **G**) We injected Cre-dependent halorhodopsin (AAV-EF1a-DIO-eNpHR3.0-EYFP) into the sensorimotor striatum of PV-Cre mice. GFP staining showing FSIs in the striatum infected with halorhodopsin (fiber only PV-Cre control: n = 4, DIO-eNpHR3.0: n = 6). **H**) A representative control mouse and DIO- eNpHR3.0 mouse. Only DIO-eNpHR3.0 mice showed transiently increased distance error during pursuit as a result of photo-stimulation (500 ms). **I)** Population summary data. Photo-stimulation immediately increased distance error during pursuit (Repeated measures two-way ANOVA, Interaction: $F(2,16) = 5.365$, $p < 0.05$, Time: $F(2,16) = 5.219$, $p < 0.05$, Group: $F(1.16) = 6.519$, $p < 0.05$; Boferroni post-hoc: Pre-stim NS, Stim NS, Post-stimulation NS, $p < 0.001$). **J)** In DIO-eNpHR3.0 group, velocity increased during photo-stimulation and decreased afterewards. Repeated two-way ANOVA: Interaction: $F(2,16) = 14.75$, $p < 0.001$, Time: $F(2,16) = 3.393$, $p = 0.0591$, Group: $F(1, 16) = 0.80$, $p = 0.3958$, Boferroni post-hoc: Pre-stim ns, Stim $p < 0.05$, Post-stim $p < 0.001$. *** $P < 0.001$. **K)** Photo-stimulation has no effect on % time spent following ($p = 0.22$) and **L)** average velocity ($p = 0.18$).

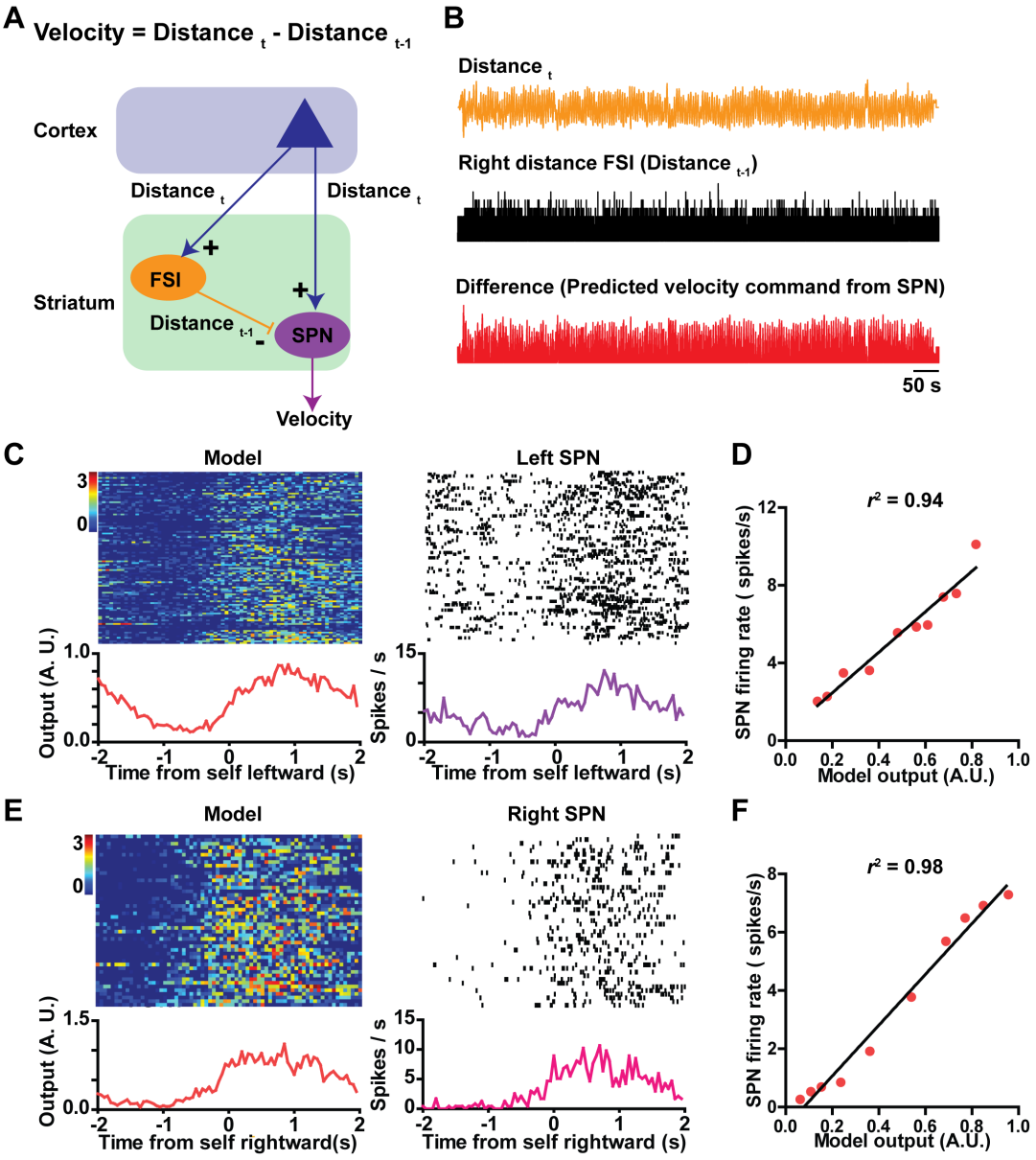

Figure 7. Working model of how FSI-SPN circuit contributes to continuous pursuit

A) Schematic diagram of the FSI-SPN feedforward inhibition circuit. Note that in the equation for velocity, distance refers to distance to target. This equation only applies to self-velocity during continuous pursuit. As shown here, excitatory cortical inputs reach both the FSI and SPN. In this case, some excitatory input represents distance to target, a key error signal used to guide pursuit behavior. In addition, the FSI relays a slightly delayed version of the same signal to the SPN. Thus the delayed distance signal (Distance $_{t-1}$) is subtracted from the distance signal (Distance $_{t}$), and the SPN output reflects the difference between these two signals, i.e. the change in distance in this time step. As the feedforward inhibition circuit can function as a differentiator, the velocity command is made equal to the change in distance. Thus left distance error will be used to guide leftward velocity, and right distance error will be used to guide right velocity error. **B)** Actual traces from our experiments illustrating the variables used in the model. **C)** The

model is compared with actual data using simultaneously recorded left distance FSI and left velocity SPN. Using actual distance measure as an estimate of the Distance $_{t}$ signal (shifted by 100 ms to account for the delay in the perceptual system) sent to the striatum, and FSI activity as the measure of the Distance $_{t-1}$ signal sent to the SPN, a subtraction generates a difference signal that is compared to the activity of an actual left velocity SPN. **D)** High correlation between model output and right velocity SPN output, $p < 0.0001$. **E)** The model is compared with actual data using simultaneously recorded right distance FSI and right velocity SPN. **F)** High correlation between model output and right velocity SPN output, $p < 0.0001$.

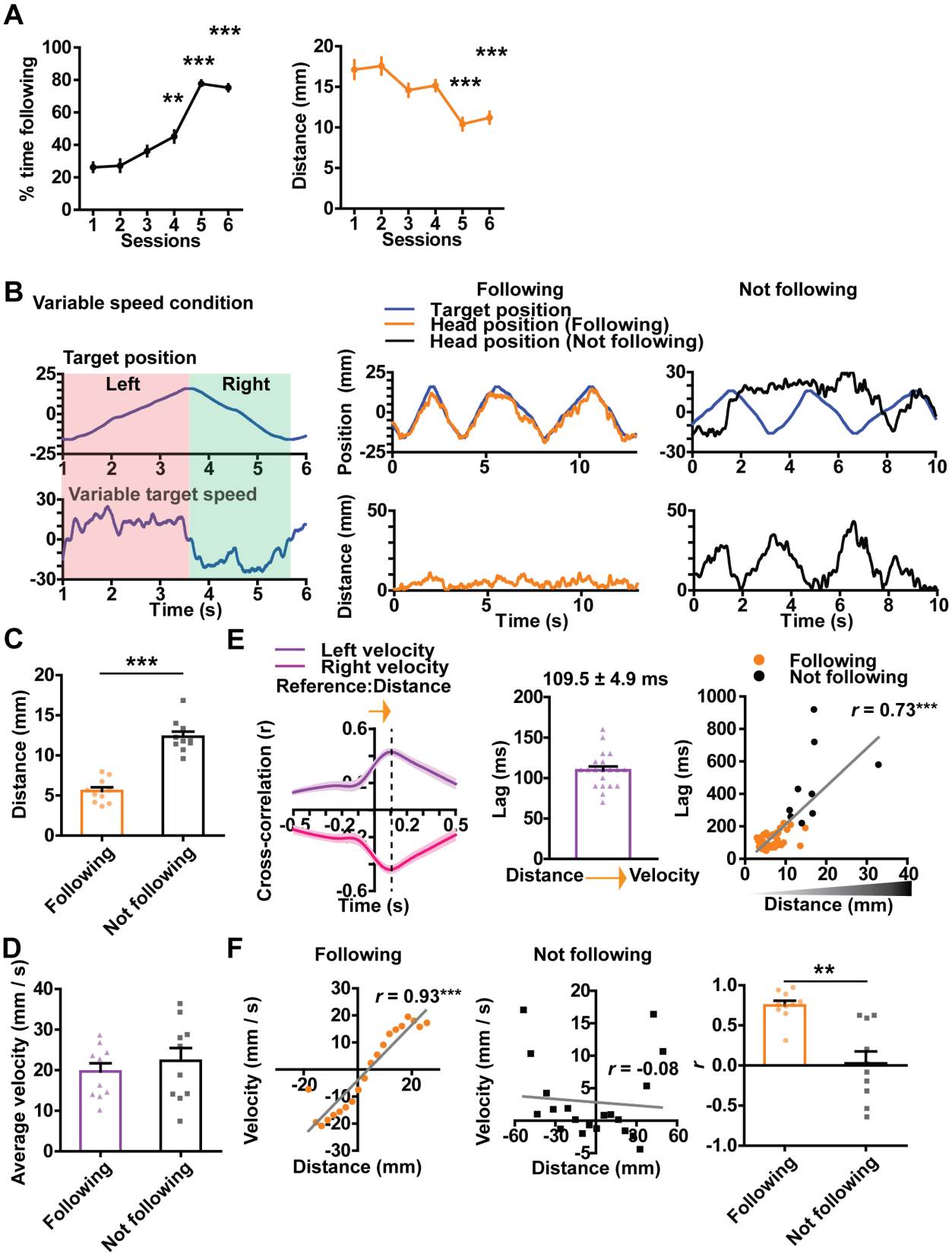

Figure S1. Summary of pursuit behavior: acquisition and variable target velocity

A) In 6 mice, we recorded behavior with 3D motion capture during training. Behavioral performance improved in the course of training. Time spent following the target increased significantly (Repeated measures ANOVA, main effect of sessions, $F(5,35) = 59.10$, $p < 0.0001$). Distance error is reduced in the same period (Repeated measures ANOVA, main effect of sessions, $F(5,35) = 16.76$, $p < 0.0001$). **B)** Representative traces of mouse head and target position during a session. Left panel shows the head and target positions during 'Following.' Right panel shows the head and target positions during 'Not following' in which two positions are different. **C)** Self-target distance error is significantly lower during following than not following (paired t-test, $p < 0.0001$). Error bars indicate ± s.e.m. *** $p < 0.0001$. **D)** Average velocity is similar between following and not following ($p = 0.053$). **E)** Illustration of the temporal relationship between distance and self-velocity. Cross correlation analysis reveals the lag between these two variables, showing that distance leads self-velocity during pursuit behavior. In addition, the lag shows a positive correlation with distance ($r = 0.73$, $p < 0.0001$). When the mouse is actively pursuing and maintaining a small distance, the lag between distance and velocity is small, but the lag increases as pursuit performance declines. Variable velocity condition. Dashed line indicates the time of peak positive and negative correlation. Shaded areas indicate ± s.e.m. **F)** Self-velocity as a function of distance to target (pursuit error). Mice use distance information to generate the appropriate velocity only during following.

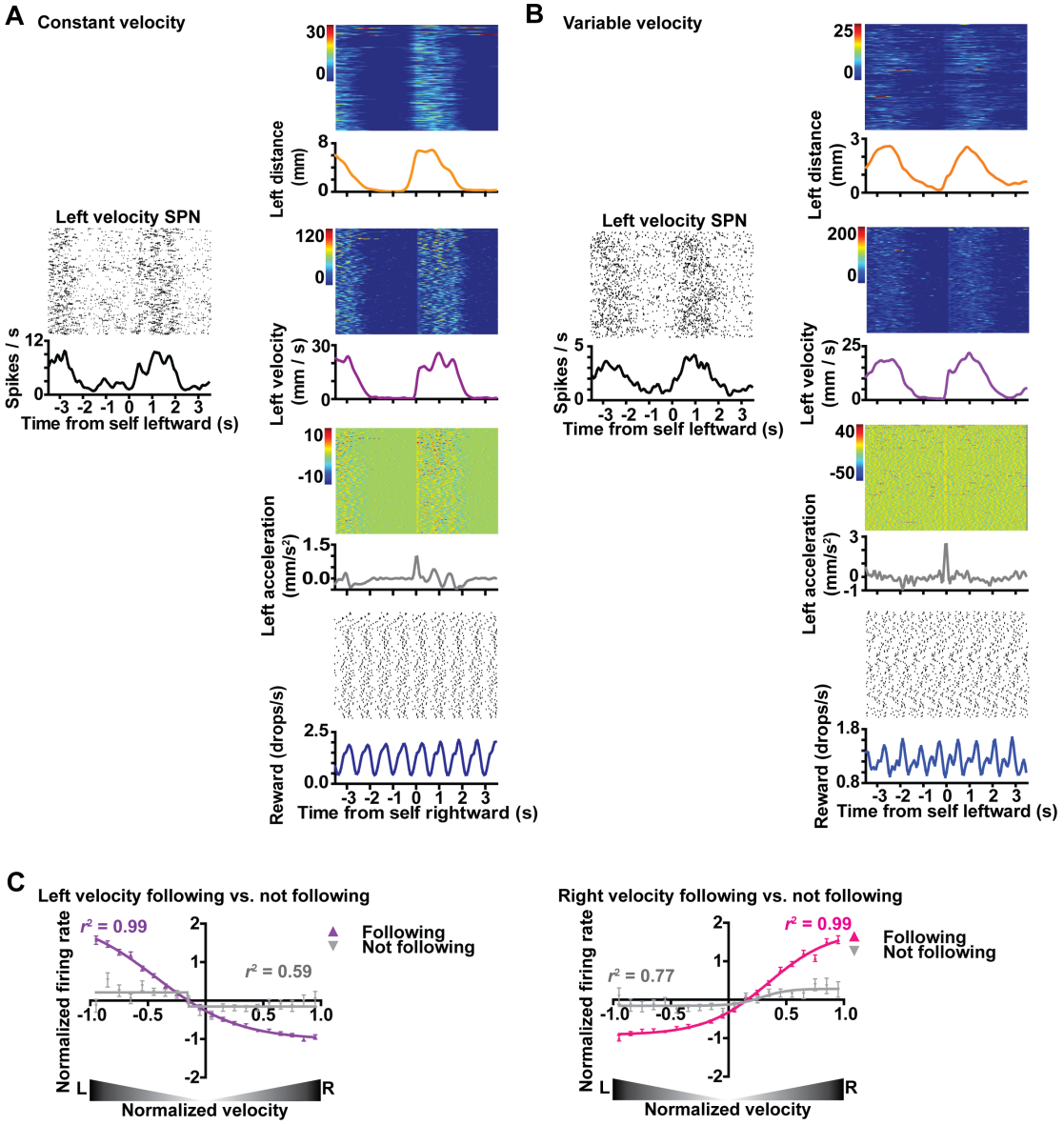

Figure S2. Representative velocity-correlated SPNs

A) In constant target velocity condition, correlation between a representative left velocity SPN and different behavioral variables (distance, velocity, acceleration, and reward). **B)** In variable target velocity condition, correlation between a representative left velocity SPN and different behavioral variables. **C**) Population summary of all left velocity and right velocity SPNs: correlation is much higher during following.

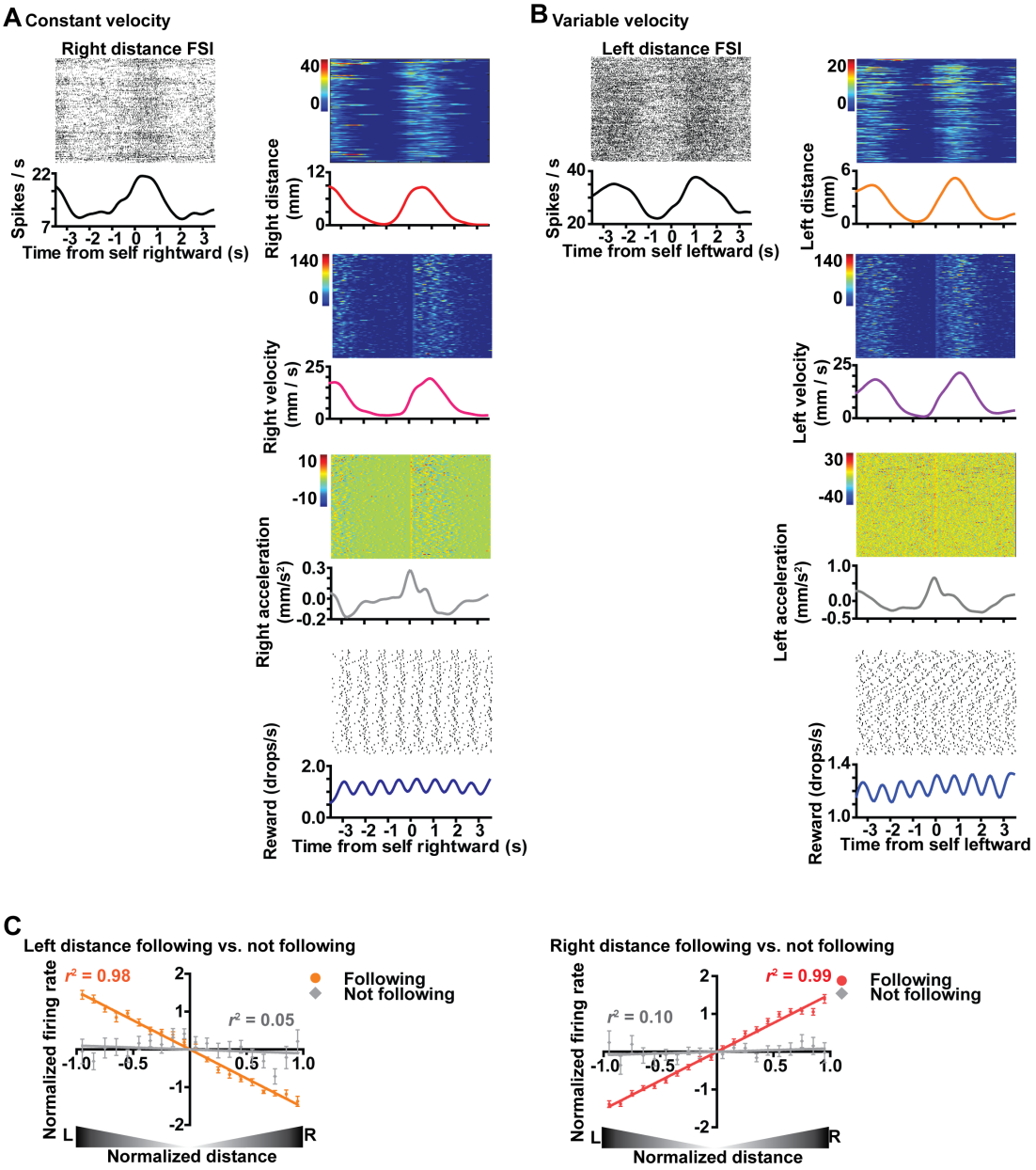

Figure S3. Representative distance FSIs and alternative behavioral variables

A) In constant target velocity condition, correlation between a representative right distance FSI and different behavioral variables (distance, velocity, acceleration, and reward). **B)** In variable target velocity condition, correlation between a representative left distance FSI and different behavioral variables. **C**) Population summary of all left distance FSIs and right distance FSIs: correlation is much higher during following.

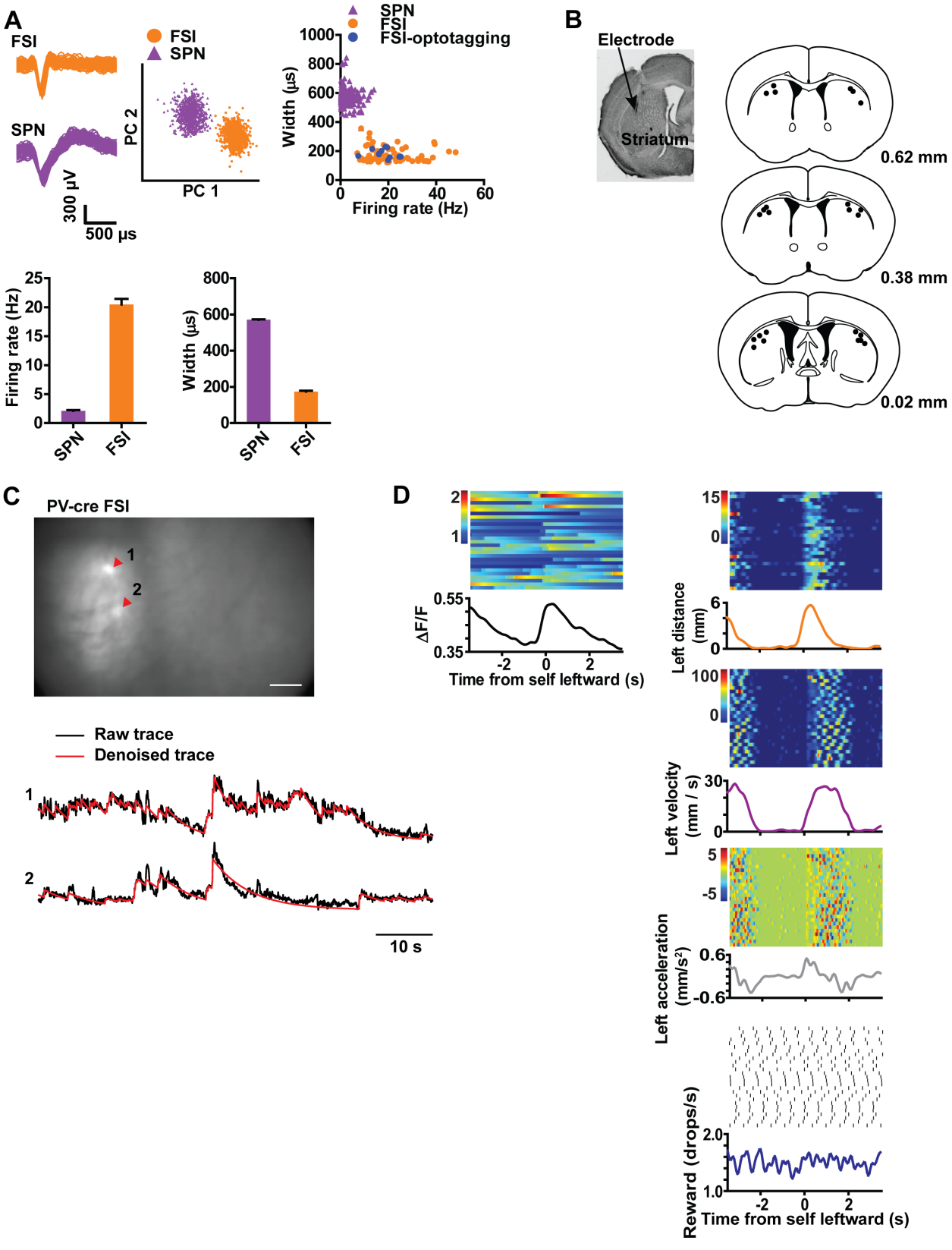

Figure S4. Summary of *in vivo* electrophysiology and calcium imaging

A) SPN and FSI have distinct waveforms and firing rates. Representative waveforms of FSI and SPN and PCA of these two cell types. FSI has significantly narrower spikes (unpaired t-test, $p < 0.0001$). *** $p < 0.0001$, and higher firing rates (unpaired t-test, $p < 0.0001$). Error bars indicate ± s.e.m. **B)** Left, representative coronal section showing location of chronically implanted electrodes. Right, estimated locations of electrodes in all mice. **C)** GCamp6s expressed in PV+ FSI in the sensorimotor striatum (red triangles). Bottom, raw traces and denoised traces estimated by CNMF method. **D)** Representative plots of a left distance FSI and different behavioral variables.

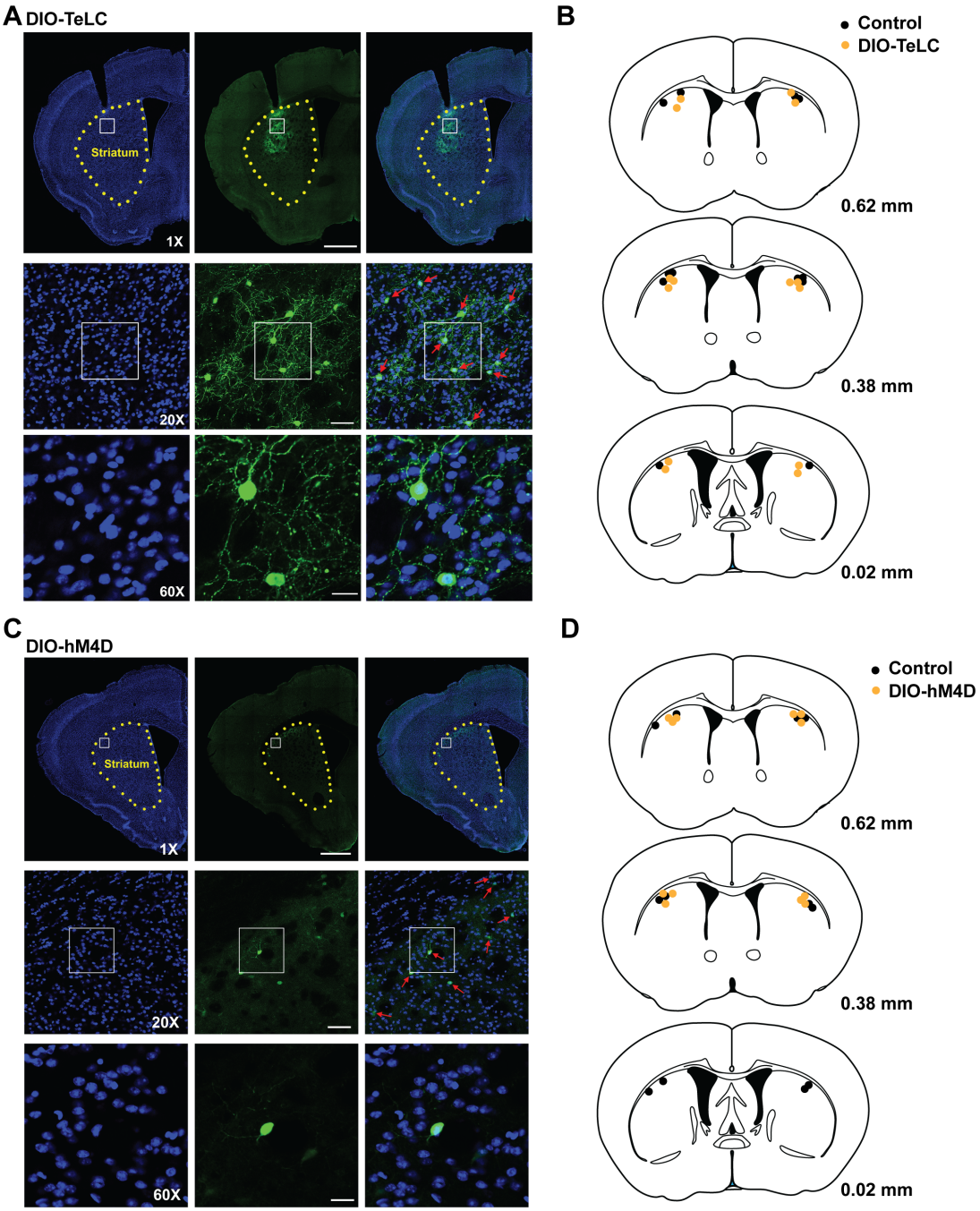

Figure S5. Summary of histology for TeLC and DREADD experiments

A) Representative expression of GFP-tagged TeLC in the striatum. **B)** Summary of TeLC expression. **C)** Representative expression of GFP-tagged hM4Di. **D)** Summary of hM4Di expression.

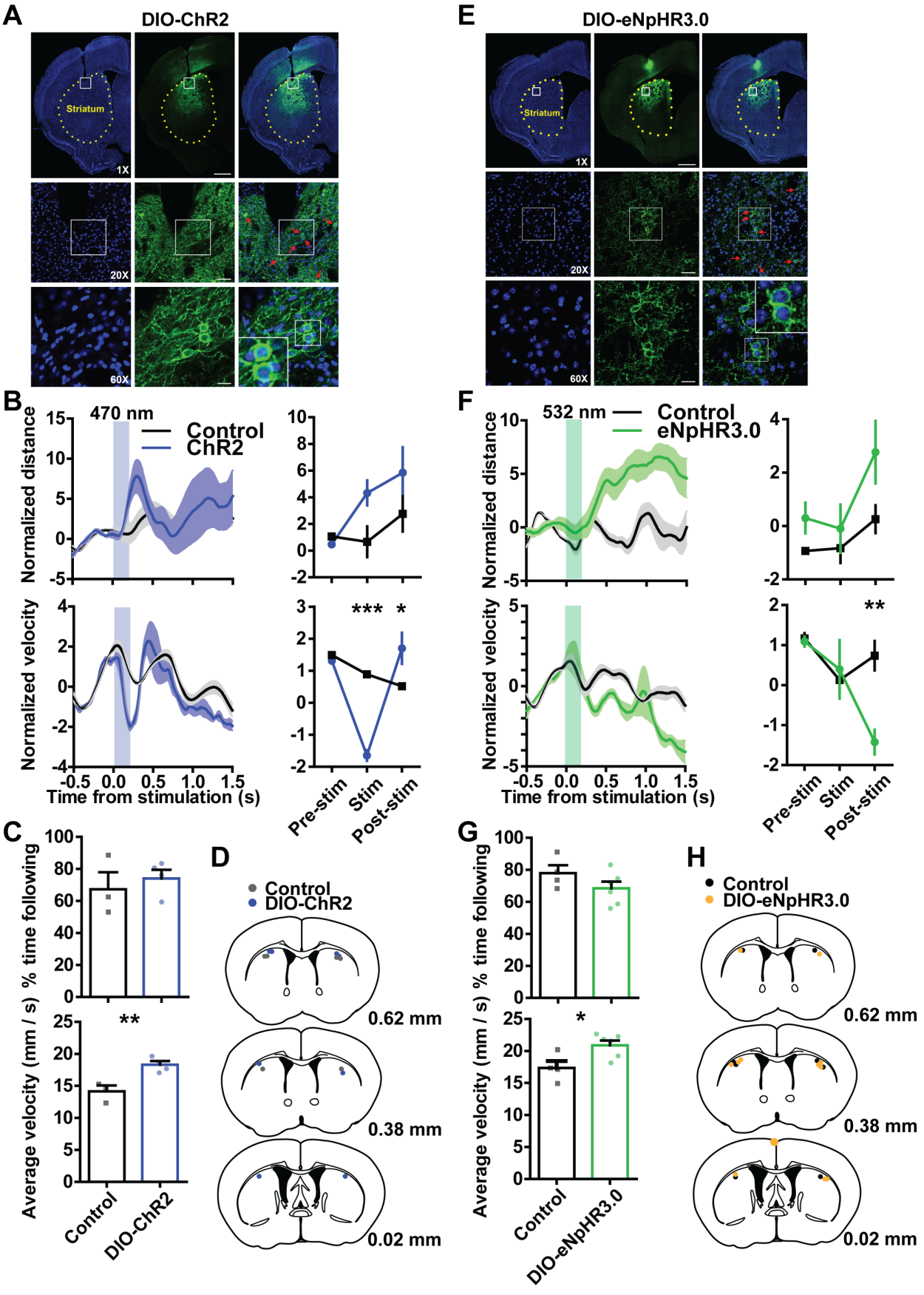

Figure S6. Summary of optogenetic experiments

A) Expression of DIO-ChR2 in the sensorimotor striatum. **B)** Population summary of stimulation (200 ms). Stimulation did not significantly affect distance error (repeated measures two-way ANOVA, Interaction: $F(2,10) = 2.968$, $p = 0.09$, Time: $F(2,10) = 6.98$, $p < 0.05$, Group: $F(1.10) = 2.49$, $p = 0.17$). DIO-ChR2 group shows reduced velocity during photo-stimulation and increased velocity after photo-stimulation. Control shows no change (Repeated two-way ANOVA, Interaction: $F(2,10) = 21.23$, $p < 0.001$, Time: $F(2,10) = 21.78$, $p < 0.001$ Group: $F(1.10) = 12.31$, $p < 0.05$, Boferroni post-hoc: Pre-stim NS, Stim $p < 0.001$, Post-stim $p < 0.05$, *** $P < 0.0001$, * $P < 0.05$). **C)** Stimulation had no effect on % time spent following ($p = 0.56$) and increased average velocity ($p < 0.01$). **D)** Estimated locations of electrodes in all mice for control and DIO-ChR2. **E**) Expression of eNpHR3.0 in the sensorimotor striatum. **F)** Population summary data. Photo-stimulation had no effect on distance error during pursuit (Repeated measures two-way ANOVA, Interaction: $F(2,16) = 1.153$ $p < 0.34$, Time: $F(2,16) = 6.654$, $p < 0.01$, Group: $F(1.16) = 2.349$, $p = 0.16$. In DIO-eNpHR3.0 group, velocity increased during photo-stimulation and decreased afterewards. Repeated two-way ANOVA: Interaction: $F(2,16) = 5.12$ $p < 0.05$, Time: $F(2,16) = 6.512$ $p < 0.01$, Group: $F(1, 16) = 2.29$, $p = 0.16$, Boferroni post-hoc: Pre-stim NS, Stim NS, Post-stim $p < 0.01$. ** $P < 0.001$. **G)** Stimulation had no effect on % time spent following ($p = 0.18$) and increases average velocity ($p < 0.05$). **H**) Estimated locations of electrodes in all mice for control and eNpHR3.0.

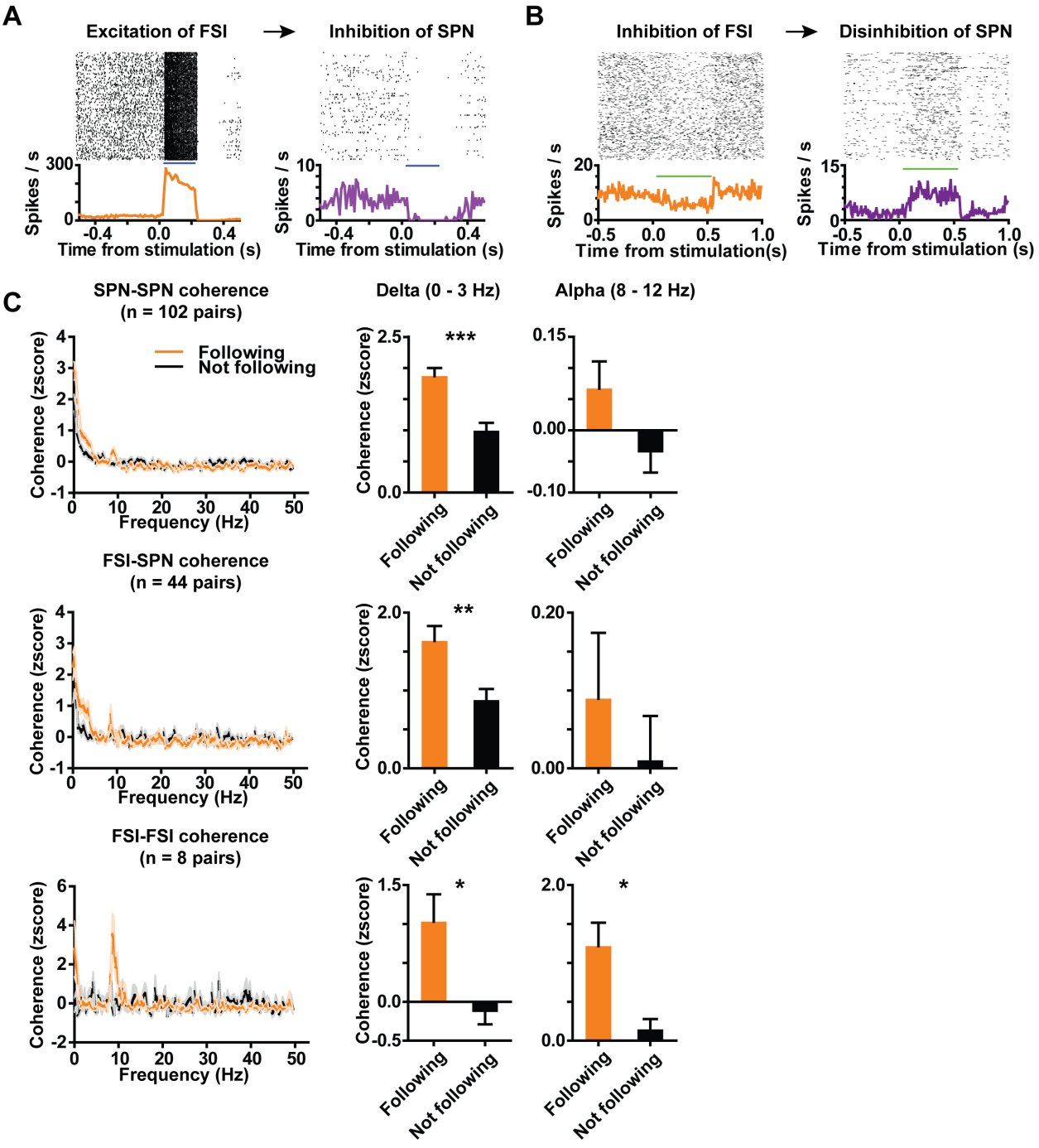

Figure S7. Summary of FSI-SPN interactions.

A) Left, excitation of FSI with ChR2 in vivo. In the same mouse, there is disinhibition of SPNs, as shown on the right. **B)** Inhibition of FSI with eNpHR3.0 and a disinhibited SPN recorded from the same mouse. **C)** Population coherence is altered during pursuit. During following, coherence is higher in alpha and delta bands.

Table 1. SPN electrophysiology summary

	Distance (n)	Velocity (n)	Acceleration (n)	Reward (n)	Unclassified (n)	Total (n)
# of neurons	5.2% (19)	32.0% (116)	3.3% (12)	0.0% (0)	59.4% (215)	100.0% (362)

	Left striatum (n)	Right striatum (n)
Left distance	2.3 % (5)	1.4 % (2)
Right distance	3.2 % (7)	3.6 % (5)
Left velocity	19.8 % (44)	10.7 % (15)
Right velocity	11.3 % (25)	22.9 % (32)
Left acceleration	1.4 % (3)	1.4 % (2)
Right acceleration	2.3 % (5)	1.4 % (2)
Reward	0.0% (0)	0.0% (0)
Unclassified	59.9 % (133)	58.6 % (82)
Total	100.0 (222)	100.0 (140)

Table 2. FSI electrophysiology summary

	Distance (n)	Velocity (n)	Acceleration (n)	Reward (n)	Unclassified (n)	Total (n)
# of neurons	56 % (51)	11.0 % (10)	5.5 % (5)	0.0% (0)	27.5 % (25)	100.0% (91)

	Left striatum (n)	Right striatum (n)
Left distance	22.9 % (11)	20.9 % (9)
Right distance	20.8 % (10)	48.8 % (21)
Left velocity	10.4 % (5)	4.7 % (2)
Right velocity	2.1 % (1)	4.7 % (2)
Left acceleration	2.1 % (1)	0.0 % (0)
Right acceleration	6.3 % (3)	2.3 % (1)
Reward	0.0 % (0)	0.0 (0)
Unclassified	35.4 % (17)	18.6 % (8)
Total	100.0 (48)	100.0 (43)

Table 3. FSI optotagging summary

	Distance (n)	Velocity (n)	Acceleration (n)	Reward (n)	Unclassified (n)	Total (n)
# of neurons	73.3 % (11)	6.7 % (1)	0.0 % (0)	0.0 % (0)	20.0 % (3)	100.0% (15)

Table 4. Calcium imaging summary

	Distance (n)	Velocity (n)	Acceleration (n)	Reward (n)	Unclassified (n)	Total (n)
# of neurons	51.4% (19)	18.9% (7)	0.0% (0)	0.0% (0)	29.7% (11)	100.0% (37)

	Left striatum (n)	Right striatum (n)
Left distance	25.9% (7)	80.0% (8)
Right distance	14.8% (4)	0.0% (0)
Left velocity	25.9% (7)	0.0% (0)
Right velocity	0.0% (0)	0.0% (0)
Left acceleration	0.0% (0)	0.0% (0)
Right acceleration	0.0% (0)	0.0% (0)
Reward	0.0% (0)	0.0% (0)
Unclassified	33.3% (9)	20.0% (2)
Total	100.0% (27)	100.0% (10)